ACS OMEGA

Open Access

http://pubs.acs.org/journal/acsodf

Review

Surface Treat Method to Improve the Adhesion between Stainless Steel and Resin: A Review

Bing Du,* Xinyu Zhou, Qichang Li, Jingwei Liu, Yuxi Liu, Xianjun Zeng, Xiangrong Cheng, and Hanjie Hu*

Cite This: *ACS Omega* 2023, 8, 39984−40004

Read Online

ACCESS | Metrics & More | Article Recommendations

ABSTRACT: Combining metal and polymer into hybrid composite materials is finding increasing interest in many industries. Special attention is being paid to increase the adhesion between the metal and polymer interface. In this paper, the current research progress of surface treatment methods for improving the interfacial adhesion of stainless steel and resin is reviewed. It involves the stainless steel surface treatment method, resin surface treatment method, and adhesion test methods of stainless steel and resin. The methods of improving the interfacial adhesion of stainless steel and resin are summarized and prospected according to the research status.

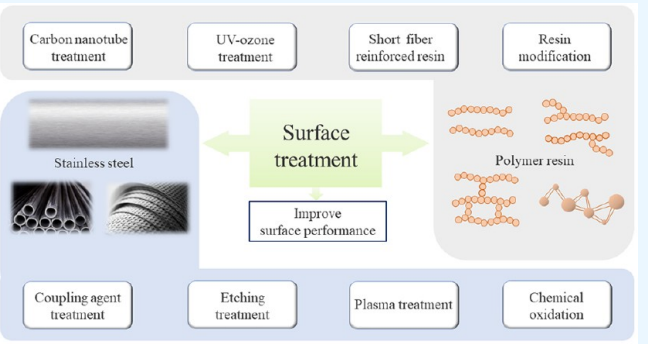

1. INTRODUCTION

Resin−matrix composites are frequently utilized in the maritime, aerospace, shipping, medical, automotive, and other fields due to their low weight and high strength characteristics.[1−8] Lightweight constructions with dependable structural strength can be fabricated using hybrids of stainless steel and resin-based composites.[9] The interfacial adhesion of the stainless steel and the resin directly affects the load-bearing capacity of composite components. The bonding process is one of the most significant aspects of bonding between composite parts and different composite structures using distinct bonding processes.[10] In order to improve the load-carrying capacity of composite materials, it is necessary to design and embed stainless steel parts in the joint part of the composite material's load-bearing structure.[11] The excellent mechanical properties of the interface between stainless steel and composite materials mostly depends on its interlayer-bonding properties.[12,13] When the interfacial bond between stainless steel and resin is strong, the load can be successfully transferred from the matrix to the stainless steel without causing damage to any component. Therefore, improving the interfacial adhesion between stainless steel and resin is the key to prepare composites with high performance.[14]

The adhesiveness of stainless steel and resin directly affects the load-bearing capacity of composite components. Although the resin can effectively penetrate the stainless steel surfaces, its low adhesion severely limits its use. Many different surface treatment methods are used to change the surface of the substrate to solve the above problems. The methods include changing the surface roughness of the substrate or the chemical properties of the substrate surface, thus improving the interfacial adhesion of stainless steel and resin. Sandblasting treatment,[15] mechanical grinding treatment,[16] chemical oxidation treatment, etching treatment,[17,18] plasma treatment,[19] and coupling agent treatment methods are frequently used procedures for stainless steel surface treatment. Sandpaper sanding and carbon nanotube modification, resin modification, and fiber reinforcement are typical techniques for treating resin surfaces. The surface treatment methods are shown in Figure 1.

For stainless steel, the surface will be affected by biofouling, resulting in undesirable results on the surface of the material. Bezek et al.[20] studied glucose concentration, temperature, and stainless steel surface roughness on biofouling by four common pathogens. It was indicated that 3D polished, brushed, or electropolished stainless steel is less susceptible to biological contamination than untreated stainless steel, and when the temperature is 4 °C, psychrophilic biofouling is still inhibited. In general, for the stainless steel and resin interface, the higher the bond strength, the better the mechanical properties of the material obtained. Generally speaking, the mechanical characteristics of the material are improved the stronger the

Received: August 4, 2023
Accepted: October 5, 2023
Published: October 18, 2023

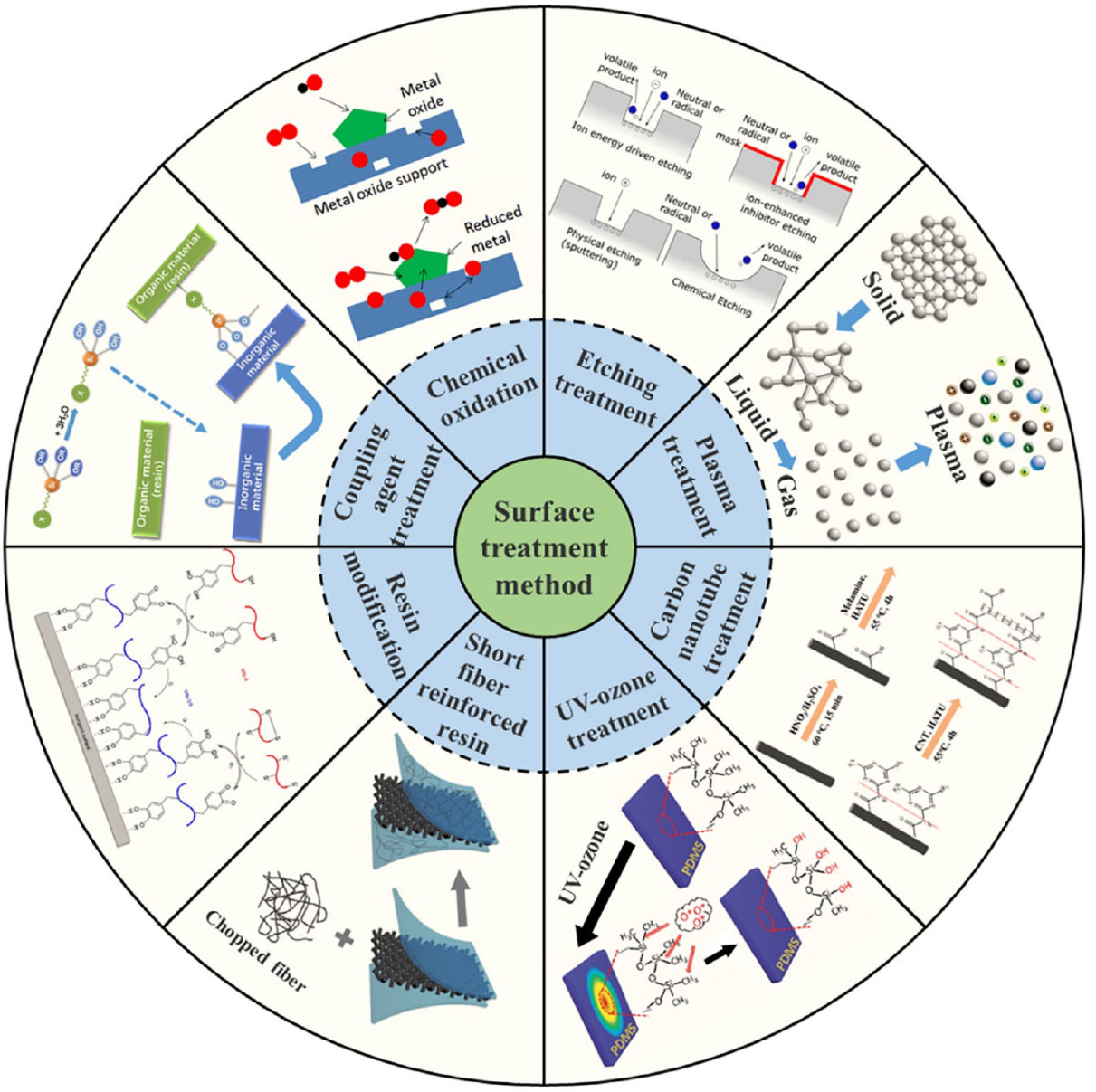

Figure 1. Surface treatment method.

connection is at the stainless steel and resin contact. The interlaminar characteristics of composite components are examined with monofilament pull-out, lap tests, and fracture toughness. Based on the above, this paper first introduces the stainless steel and resin surface treatment methods, respectively. Subsequently, the test method of stainless steel and resin adhesion is introduced. Finally, the current status of research on the methods to improve the adhesion of stainless steel and resin is summarized.

2. SURFACE TREATMENT METHOD OF STAINLESS STEEL

Stainless steel has the advantages of high strength, heat resistance, corrosion resistance, and resistance to rust. The interfacial adhesion of stainless steel and resin can be improved by enhancing the surface roughness and surface wettability of stainless steel. Table 1 summarizes the published work on surface treatment of stainless steel.

2.1. Surface Roughness. An appropriate enlargement in stainless steel surface roughness can increase the contact area between stainless steel and resin, thus improving the adhesion between stainless steel and resin. Surface treatment has been widely used to improve the surface roughness of stainless steel. To improve the surface state of stainless steel, surface silanization, oxidation treatment, chemical etching, etc., are often applied.

2.1.1. Surface Silanization. Silane coupling agents are reactive to inorganic materials due to their silicone alkoxy groups and reactivity or compatibility with organic materials due to their organic functional groups. Silanization modification contains functional groups that can provide stainless steel with a more electrically stable surface. This can help minimize static charge buildup. Silanization modification of stainless steel increases the surface roughness between stainless steel and polymer, thereby improving the interfacial adhesion. In addition, silanization modification can improve the surface

https://doi.org/10.1021/acsomega.3c05728
ACS Omega 2023, 8, 39984−40004

Table 1. Stainless Steel Surface Treatment Method Summary

improvement method	surface treatment	performance test methods	results	ref
increase surface roughness	silane coating	single-lap shear	An oxidation temperature of 500 °C with ethanol as solvent and a solution pH of 11 was used to obtain the best LSS.	22
	immersion in 10% ethanol solution of silane in different proportions of MEMO:A-1110	XPS analysis	Surface binding energy of 284.6, 286.3, and 288.5 eV for MEMO and A-1110 coated, respectively, was obtained.	23
	immersion in 5:5:90 solution of A-1387 silane hydrolysis	tensile shear test	The tensile shear strength was greatly improved by the addition of coupling agent.	24
	immersion in hydrolyzed APS solution	pull-off test	SS/epoxy resin fracture strength increased to 60 MPa after silane coupling agent treatment.	25
	APTES silane grafting	pull-off test	IFSS increased by 36% to 38 MPa.	26
	immersion of silane coupling agent WD-50 hydrolyzed at different mass fractions	pull-off test	Tensile strength peaked at 1.5% silane coupling agent addition.	27
	microarc oxidation treatment	shearing experiment	The maximum shear strength of 33.20 MPa was achieved at an oxidation time of 30 min.	29
	surface oxidation process	shearing experiment	The shear strength was increased by 116% and 130% by oxalic acid oxidation and oxalic acid/sulfuric acid oxidation, respectively.	30
	electrochemical anodizing treatment	SEM microscopy	Anodized SS surface roughness of 0.1560.01 nm increased to 3.8360.02 nm.	32
	chemical etching of stainless steel by immersion in HCl solution for different times	lap shear test	When immersed in HCl for 30 min, LSS obtained a maximum value of 35.44 MPa.	35
	stainless steel surface treated with 0.2 M hydrochloric acid solution	pull-off test	Tensile strength of stainless steel reached maximum after 90 min acid treatment.	37
	decompression plasma jet surface treatment with argon and nitrogen gas mixture	pull-off test	The adhesion of the specimens improved after plasma jet treatment and showed a strong Lr dependence.	40
surface wettability	in situ growth of carbon nanotube (CNT) by flame method on stainless steel surface	shear strength test	CNT growth time of 10 min was obtained when the welded joint reached a maximum shear strength of 39.2 MPa.	35
	flame method to grow CNTs on stainless steel surface	single-lap shear test	The maximum tensile strength of the stainless steel mesh with a processing time of 10 min was 18.1 MPa.	45
	plasma-activated chemical vapor deposition treatment	splice shear test	PPMA as a plasma-treated lap shear strength was significantly improved.	48
	plasma activation treatment	splice shear test	After plasma activation, the adhesion strength was increased by 80% and 150%, respectively.	49
	atmospheric pressure plasma jet for surface modification	contact angle	The contact angle of steel use stainless (SUS) was greatly reduced from 49.928 to 10.92, thus increasing its wettability.	51
	immersion in different concentrations of titanate coupling agent ethyl acetate solution for 10 min	shear strength test	The shear strength of the modified phenolic adhesives was significantly higher after TMC-2 treatment. With the increase of TMC-2 concentration, the shear strength increased from 26.21 to 39.56 MPa.	53

https://doi.org/10.1021/acsomega.3c05728
ACS Omega 2023, 8, 39984−40004

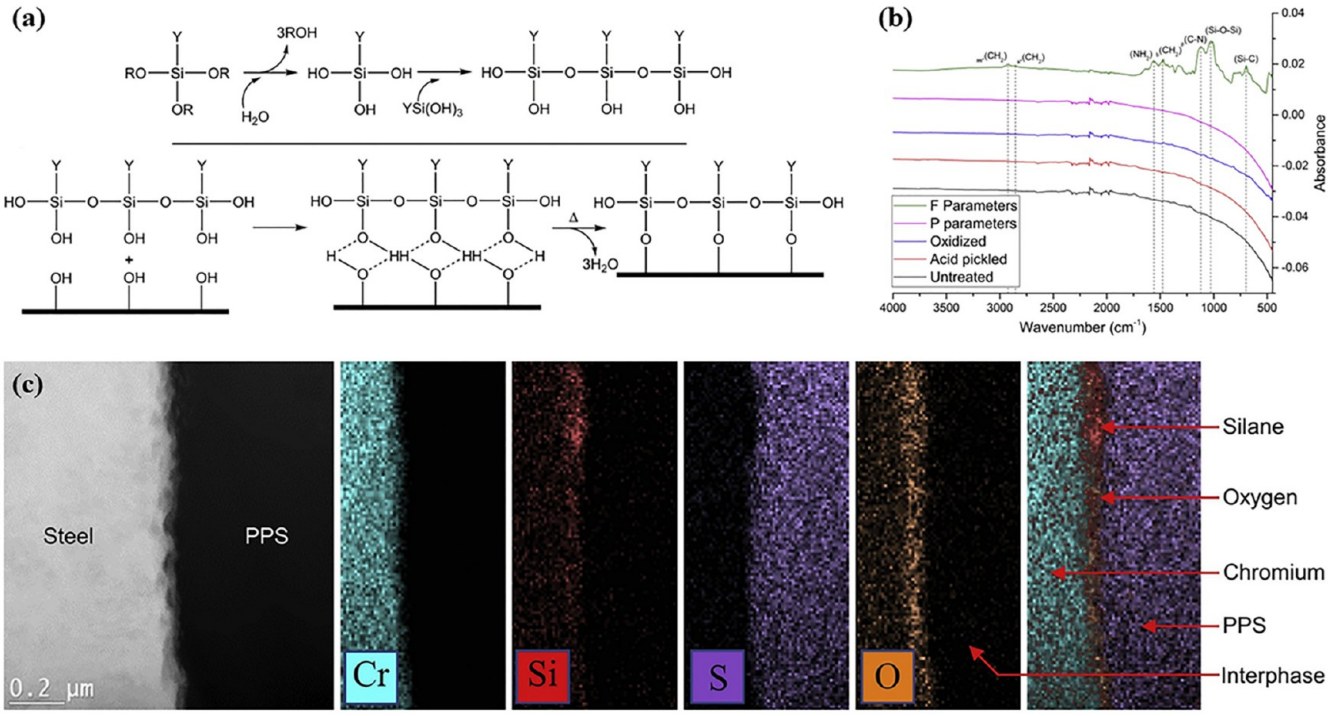

Figure 2. (a) Silane hydrolysis mechanism, (b) IR spectra of cleaned, acid-pickled, oxidized at 500 °C for 30 min, and silane-coated SS plates with parameters *P* and *F*, and (c) TEM image of the SS/PPS interface of a joint welded with a mesh coated with parameter *F*, reproduced with permission from Rohart et al. Copyright 2020, Elsevier Ltd.[22]

functionalization and contamination resistance of stainless steel.

They are commonly used to improve the bonding properties between organic and inorganic materials, whether for composite fibers, paints, or the production of metal/plastic blends for automobiles.[21] Rohart et al.[22] found that the silane molecules form oligomers with neighboring molecules according to the mechanism shown in Figure 2a. The hydroxyl molecules are formed by the hydrolysis of siloxyl groups. The oligomers condense on the surface and form covalent bonds with the surface through the hydrogen-bonding process. The ATR-FTIR spectra in Figure 2b show that the spectra of SS treated with clean, pickled, oxidized, and parameter *P* silylation do not show any peaks, and the spectra of SS treated with parameter *F* for silylation have no peaks either. It indicates that after hydrolysis the adjacent silane molecules form a siloxane network with Si−O−Si bonds. The TEM image of the SS/PPS interface of the grid-welded joint treated with parameter *F* silanization is shown in Figure 2c. Silicon and oxygen form an interface at the boundary between SS and PPS, which increases the surface roughness.

Wang[23] found that the −Si−O− functional group at one end of the hydrolyzed silane MEMO molecule could react with the hydroxyl group on the surface of stainless steel to form a stable chemical bond. The results by XPS showed that the surface bonding energies of coated MEMO and A-1110 were 284.6, 286.3, and 288.5 eV, respectively, compared with the stainless steel not treated with silane. Li[24] found that a stable chemical bond was formed between the stainless steel surface and PA6 resin in the presence of silane coupling agent.

Ghosh et al.[25] found that silane hydroxyl groups formed hydrogen bonds with metal hydroxyl groups through adsorption and silanol groups covalently linked to each other with the substrate surface. The forming of a siloxane network and metal−siloxane increased the surface roughness. Interfacial strength of the silanized SS/epoxy resin increases, and the failure mode evolves from the mixed adhesive-integrated failure to the more cohesive failure mode. Li et al.[26] studied silane coupling agent grafting treatment on the SSM surface. The stainless steel mesh surface showed a significant increase in surface roughness compared to the aryl diazo-grafted and sandblasted stainless steel surface. The treatment significantly enhanced the interfacial adhesion between the stainless steel and the PEEK substrate. The surface contact between the PEEK substrate and the stainless steel was greatly improved as a result. Yang[27] discovered that the silane coupling agent creates a filmlike interfacial layer between the ABS and the stainless steel fibers that can operate as a buffer to disperse and release the impact energy.

2.1.2. Surface Oxidation Treatment. A practical way to adjust the surface roughness of stainless steel is to apply the surface oxidation process, which comprises cathodic oxidation, microarc oxidation, and acid oxidation. The microarc oxidation method sets the metal or alloy in an aqueous solution of electrolyte. The metal acts as the anode, and the electrolyzer acts as the cathode. Through the combined action of electrochemistry, plasma chemistry, and thermochemistry, a ceramic layer with high bond strength is formed on the surface of the metal, thereby increasing the surface roughness.[28] Zhao[29] found that the microarc oxidation reaction is violent, which generates oxide film on the surface of the specimen, and there are a lot of holes in the film layer. Due to the high temperature of the microarc oxidation method, a large amount of molten material is generated around the holes, which increases the surface roughness. They evaluated the surface roughness of the specimens treated with different microarc

https://doi.org/10.1021/acsomega.3c05728
ACS Omega 2023, 8, 39984−40004

oxidation times by confocal laser equipment. The surface height diagrams of the specimens treated with different microarc oxidation times are shown in Figure 3. The result

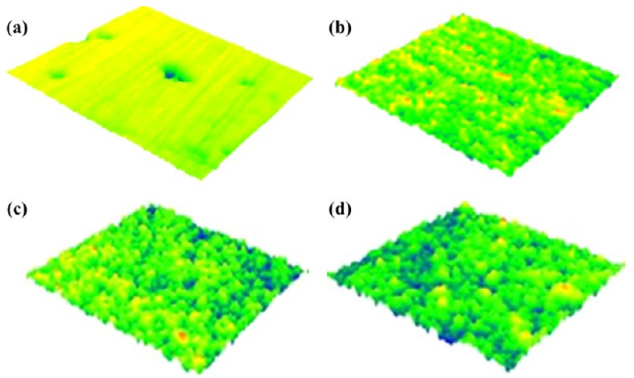

Figure 3. Surface height of specimens treated with different microarc oxidation times: (a) 0, (b) 10, (c) 20, and (d) 30 min, image courtesy of Zhao.[29]

shows that with the increase of reaction time, the diameter of micropores on the film surface increased, but the quantity declined, and the surface flatness decreased.

Acid oxidation treatment produces moderate chemical corrosion on the metal surface and changes the surface physicochemical properties, thus improving its surface roughness and exhibiting better surface adsorption. Zhou et al.[30,31] found that the surface treatment of stainless steel workpieces by hydrochloric acid oxidation or oxalic/sulfuric acid oxidation showed large uniform and continuous concave surfaces. This increases the surface roughness and yields the highest gluing shear strength. A consistent, thick oxide layer can be grown through anodizing on metals and a number of alloys. Ni et al.[32] found that the range of crater sizes increased for anodized 316L stainless steel, and the roughness increased from 0.15 ± 0.01 nm to 3.83 ± 0.02 nm as the crater size on the anodized SS surface increased. Bouquet et al.[33] found that after anodizing stainless steel, the surface porosity and the roughness increased. Gaillard and Romand[34] found that after anodizing the stainless steel surface with nitric acid electrolyte, the surface roughness increased. and the bonding performance of the stainless steel/epoxy system was greatly improved.

2.1.3. Chemical Etching. Oxide layer is a quick, flexible form of surface modification that offers high precision, high speed, and customizable etching depth. When stainless steel mesh is used as a heating element, the surface of the stainless steel mesh can be optimally designed by chemical etching methods. This method significantly improves the bonding properties at the weld interface, increasing the strength of the welded joint. Zhao[35] studied the chemical etching of the stainless steel mesh surface using HCl solution. Figure 4a shows that the surface roughness of the stainless steel mesh increases with the growth of soaking time. Figure 4b shows that the single stainless steel wire diameter with tensile strength decreases. When t = 50 min the retention of tensile strength is about 88%. According to Figure 4c, the hydrophobicity of SS increases with t, and the contact angle suddenly increases after the time passes 20 min, reaching the maximum of 120° at 50 min.

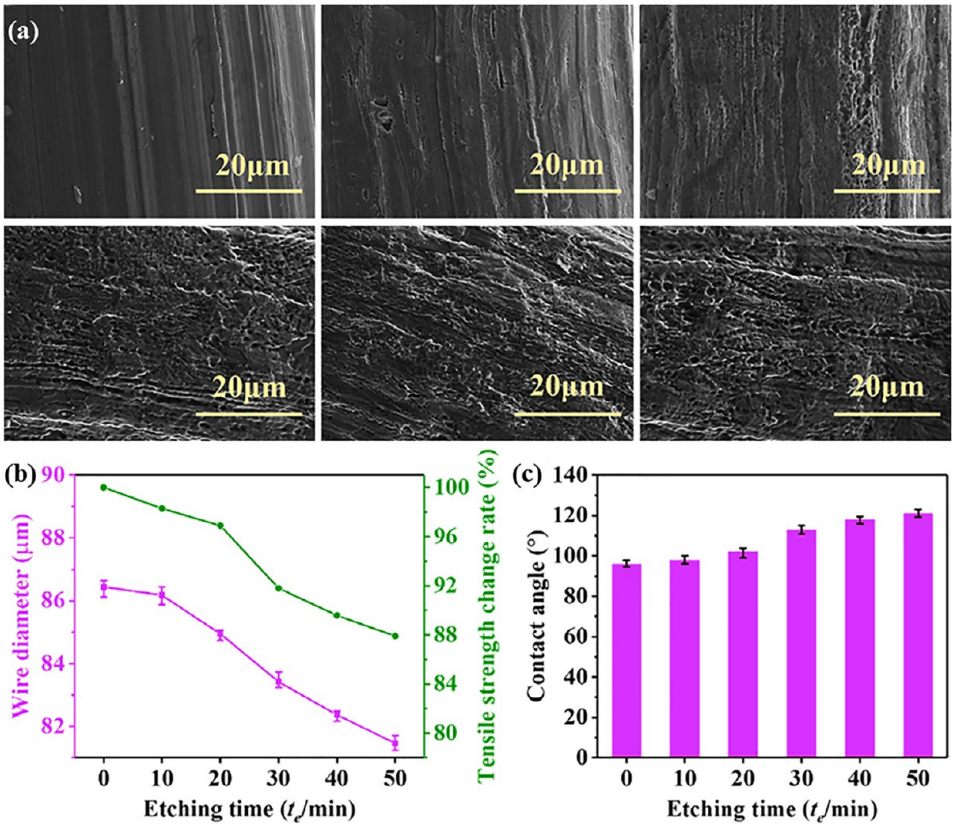

Figure 4. (a) Surface morphologies of SS mesh etched for different t_e, , (b) SS wire diameter and tensile strength retention rate for different t, and (c) contact angle of the SS wire against water, image courtesy of Zhao.[35]

https://doi.org/10.1021/acsomega.3c05728
ACS Omega 2023, 8, 39984−40004

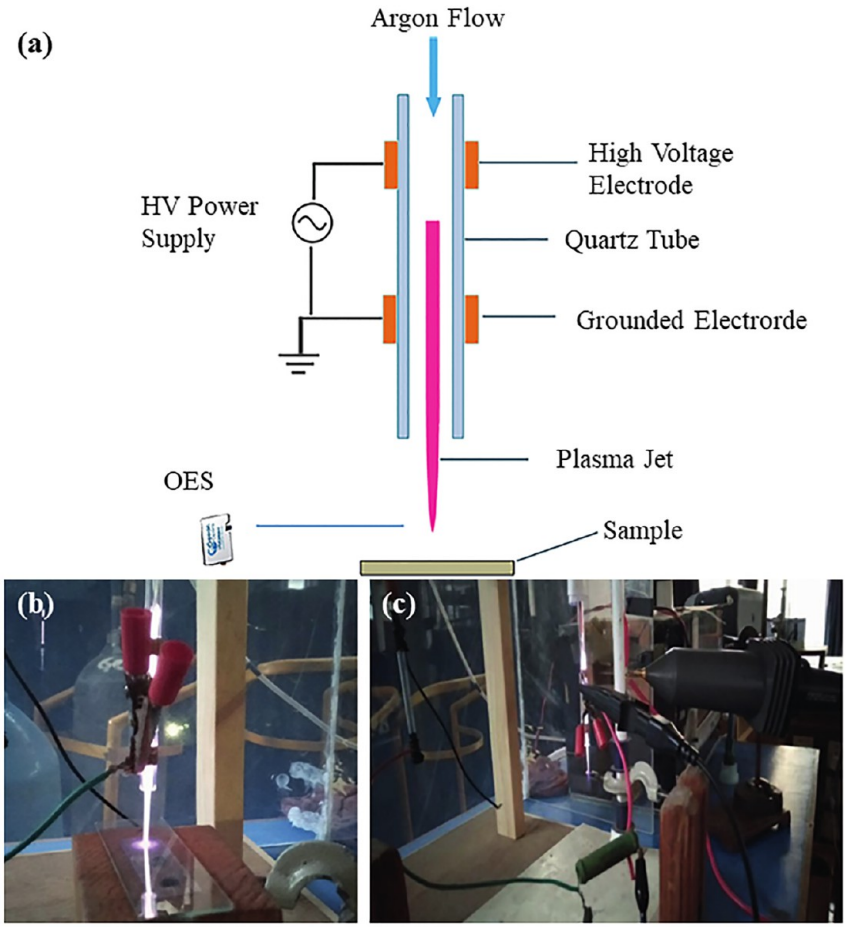

Figure 5. Schematic diagram of the experimental setup for plasma jets: (a) schematic diagram of the experimental setup for plasma jets, (b) image of the discharge (jet) during polymer treatment, and (c) image of the discharge (jet) during an electrical characterization, reproduced with permission from Baniya et al. Copyright 2021, Scrivener Publishing LLC.[39]

Stainless steel surface etching pits and roughness increased when the stainless steel grid was immersed in a hydrochloric acid solution for chemical etching.[36] However, IFSS testing could not be finished if the etching time was more than 30 min. Kwom and Lee[37] found microcracks and etching pits on the surface of acid-treated stainless steel fibers and an increase in the adhesion strength of stainless steel fibers and epoxy resin. Van Rooijen et al.[38] found etching pits on the surface of sulfuric acid−sodium dichromate-treated stainless steel sheets and an increase in the peel strength of stainless steel.

2.1.4. Plasma Jet. By plasma surface treatment technology, the material surface can be assaulted with high-energy plasma particles, thereby deteriorating the surface material and improving the surface roughness. Baniya et al.[39] employed the plasma jet experiment setup shown in Figure 5a for surface modification of polymers. The experiment procedure is shown in Figure 5b, where a plasma jet is generated between two electrodes. The experimental results show the ability to improve its surface adhesion. Chen et al.[40] found that the surface roughness of stainless steel treated with Ar−N_2 mixed gas plasma jet increased when the surface roughness was measured by a roughness meter. The plasma jet method can clean the surface of the stainless steel and reduce contaminants. The plasma has highly charged particles.[41] The adhesion of stainless steel after plasma jet treatment was significantly improved, indicating that plasma treatment has a significant effect on improving the adhesion of metal to resin.

2.2. Surface Wettability. The contact angle, denoted by the wetting theory,[42] is the angle between the tension at the gas−liquid interface and the solid−liquid interface at the intersection of the gas, liquid, and solid phases. The degree of wetting of a solid by a liquid can be inferred from the value of the contact angle. When the angle is >90°, the solid is not wet. When the angle is between 0° and 90°, the solid can be wetted, and when the angle = 0°, the liquid can wet the solid substrate; this is the optimum situation.[43] It is obvious that the wettability of the stainless steel surface increases with the decreasing of the contact angle.

2.2.1. Surface Preparation of Carbon Nanotubes. Due to the carbon nanotube (CNT) nanoreinforcement, the interfacial bond strength of composites can be enhanced by incorporating the CNT into their interfaces. The increased porosity of the CNT makes stainless steel more wettable. According to the microdrop tests, the CNT-grafted CF-reinforced composites demonstrated a 30% higher interfacial shear strength than the CF-reinforced composites.[44] Zhao[35] found that CNTs synthesized by the flame method used grooves as growth templates and grew as arrays on the surface of stainless steel mesh. The capillary effect of the high-porosity CNT increased the wettability of the stainless steel wire and improved the interfacial adhesion of stainless steel and PEI

https://doi.org/10.1021/acsomega.3c05728
ACS Omega 2023, 8, 39984−40004

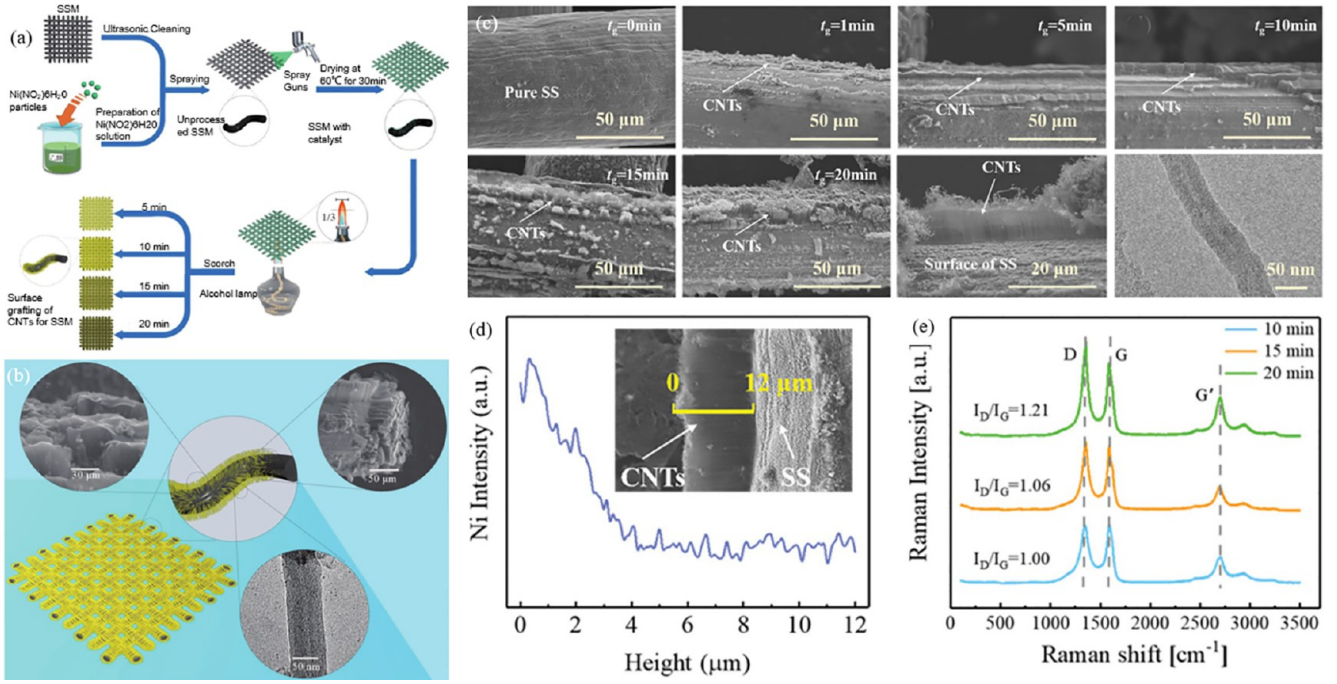

Figure 6. (a) Schematic of CNT-grafted SSM; (b) SEM and TEM micrographs of CNTs; image courtesy of Xiong et al.[45] (c) SEM images of CNTs on the SS wire, (d) EDX spectrum of nickel element intensity on the CNT array, and (e) Raman spectra of CNTs at *tg* = 10, 15, and 20 min, reproduced with permission from Xiong et al. Copyright 2021, Taylor. & Francis.[46]

resin. Xiong et al.[45,46] used the flame method to graft CNTs on the surface of stainless steel, and the experimental flowchart is shown in Figure 6a. The CNTs can grow an overall ordered fir tree structure of CNTs by continuous accumulation of neighboring, short-term, crowded catalyst sites, as shown in Figure 6b. Figure 6c shows that the CNTs grow vertically in a nonuniform array on the surface of the SS lines. According to Figure 6d, the content of nickel elements decreases sharply from the top to the bottom of the CNTs array. Figure 6e shows the Raman spectroscopy plot, where the value of ID/TG reaches 1.21 when *t* reaches 20 min. The capillary effect of the high-porosity CNTs arrays improves the wettability of stainless steel and enhances the interfacial capability of stainless steel and resin.

2.2.2. Plasma Treatment. Positive and negative ions, electrons, and free radicals in the plasma can realize plasma−surface interactions.[47] Ochoa-Putman and Vaidya[48] found that the treatment of metal surfaces with plasma-activated chemical vapor deposition (PACVD) decreased the water contact angle and increased their surface wettability. Williams et al.[49] found that the water contact angle of 410 stainless steel reduced after He/O_2 plasma treatment. The surface wettability was increased, and the adhesion of bonded stainless steel specimens was increased by 50%. Kim et al.[51] studied the surface modification of stainless use steel (SUS) using an atmospheric pressure plasma jet. The contact angle of SUS was greatly reduced from 49.928° to 10.92°, which increased its wettability.

2.2.3. Resin Precoating. The resin-precoated stainless steel surface can effectively improve the wettability of stainless steel. Wang et al.[52] precoated the steel substrate surface with resin, as shown in Figure 7a. The resin precoat can improve the wettability of the stainless steel through removing micro-porosity, thus improving the interfacial adhesion. Figure 7b compares the epoxy resin droplets on different substrate surfaces, and the improvement in wettability is evident. The effect of different surface treatments on the bond strength was tested by single-lap shear (SLS). Figure 7c shows that the interfacial shear strength increased by 57% for the 10 wt % resin−acetone solution for precoating.

2.2.4. Titanate Coupling Agent Treatment. It has been amply demonstrated that the titanate coupling agent in thermoplastics, thermosets, rubber, and other filler systems improves the compatibility of organic and inorganic materials. Zhu et al.[53] treated the stainless steel with bis(dioctyl pyrophosphate) ethylene titanate (TMC-2). The polar portion of its solid surface energy was reduced, and the contact angle between the hydrophobic stainless steel surface and the phenolic binder was lower, resulting in increased wettability. The adhesion strength rose from 26.21 to 35.37 MPa as the phthalate coupling agent concentration increased, peaking at 39.56 MPa at a concentration of 2%.

3. SURFACE TREATMENT METHOD OF RESIN

The interfacial adhesion of stainless steel and resin can be enhanced by improving the flow of resin, short-cut fiber-reinforced resin, and resin modification. The published research on resin surface treatment is listed in Table 2.

3.1. Resin Fluidity. By combining resin with carbon nanotubes, ultraviolet (UA)-ozone treatment, and resin, resin flow can increase. Due to their superior mechanical qualities, the CNTs are frequently employed in the composites made from the modified polymers.[54] The CNTs are often dispersed directly into the resin as a means of altering continuous fiber-reinforced resin matrix composites. However, the performance of CNTs cannot be effectively utilized due to issues like viscosity and self-filtration effects.[55−57] Therefore, CNTs can be effectively dispersed in the resin by in situ growth or chemical grafting of CNTs onto continuous fibers. Baltzis et al.[58] found that the modification of epoxy resin by carbon

https://doi.org/10.1021/acsomega.3c05728
ACS Omega 2023, 8, 39984−40004

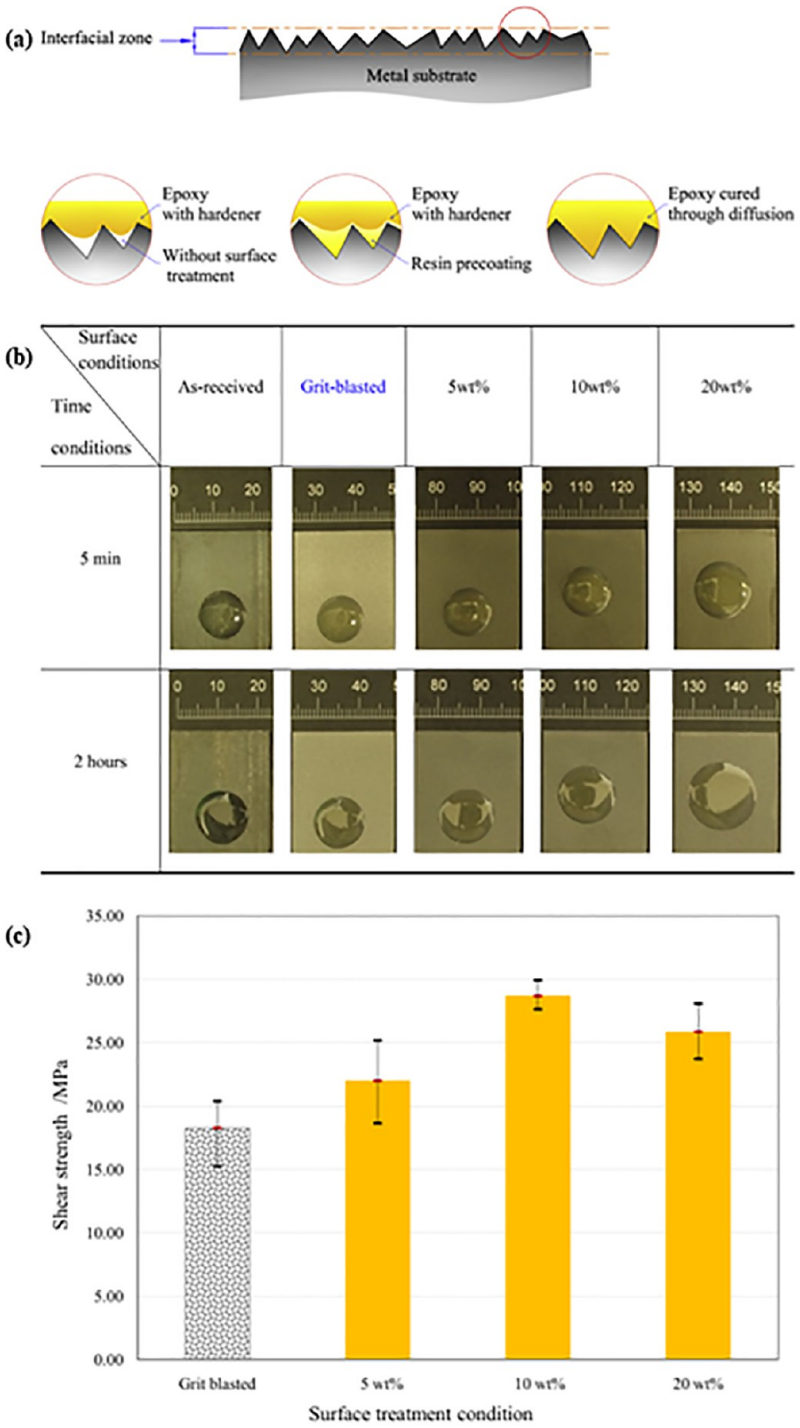

Figure 7. (a) Cross-sectional view of sandblasted steel substrate, (b) top view of small epoxy droplets on five different substrate surfaces, and (c) shear strength measured by SLS tests on the grit-blasted surfaces with 0, 5, 10, and 20 wt % of resin−acetone solutions. Reproduced with permission from Wang et al. Copyright 2016, Elsevier Ltd.[52]

nanotubes can improve its wettability to 304 stainless steel, thus significantly enhancing the bond strength of the resin to stainless steel.

Wang[23] found that mixing modified petroleum resin can improve the flowability of ethylene acrylic acid/linear low-density polyethylene (EAA/LLDPE), thus increasing its wettability to stainless steel, besides increasing the surface adhesion of EAA/LLDPE to stainless steel. Arai et al.[59] used ultraviolet (UV) ozone to pretreat the surface of cyclic olefin polymer (COP) specimens with metal. As in Figure 8a, COP was laser bonded to SUS304. Then the samples were subjected to tensile shear tests. They compared the appearance of the different pretreatment times. At 600 s, the joint interface appears yellow, which is considered to be oxidative degradation. Figure 8b shows a TEM photograph of the interface between COP and SUS304, and it can be concluded that there is a thin film of about 6 nm at the joint interface. EDX analysis shows that this film contains Cr203. Figure 8c

https://doi.org/10.1021/acsomega.3c05728
ACS Omega 2023, 8, 39984−40004

Table 2. Resin Surface Treatment Method Summary

improvement method	surface treatment	performance test methods	results	ref
resin fluidity	addition of C5/C9 petroleum resin modified by grafting with maleic anhydride	peel strength test	After adding the modified C5 petroleum resin, the peel strength before and after soaking reached 28.6N/cm and 15.2 N/m, respectively.	23
	surface pretreatment of cyclic olefin polymers(COP) using UA-ozone	microscopic observation	COP surface generated functional groups to improve the adhesion between 304 stainless steel and COP.	59
	carbon nanotube (CNT)-reinforced epoxy resin	single-lap shear	The lap strength was increased by nearly 50%, and the maximum shear strength was achieved when the CNT content in the adhesive was 0.6%.	58
short-fiber reinforcement	adding short-fiber strand to the resin solution	single-lap shear	The mechanical properties of the weld head were significantly improved, with a maximum tensile strength of 35.97 MPa.	35
	short Kevlar fiber-toughened epoxy resin	shear strength test	Further improvement of the shear strength of the glued joint was seen.	62
	short carbon fiber (SCF)-reinforced polyethylene (PE) polymer composites	shear strength test	The shear strength of SCF/PE−PE composite weld interface was 6.1%% higher than that of pure PE−PE weld interface.	64
resin modification	modification of epoxy resins with polymers containing catechol	single-turn shear test	Maximum lap shear strength increased by nearly two times.	66
	UV-treated modified thermoplastic resin matrix composites	lap shear strength	The UA treatment formed a carbonyl group, and the bonding properties of the joint were significantly improved.	68

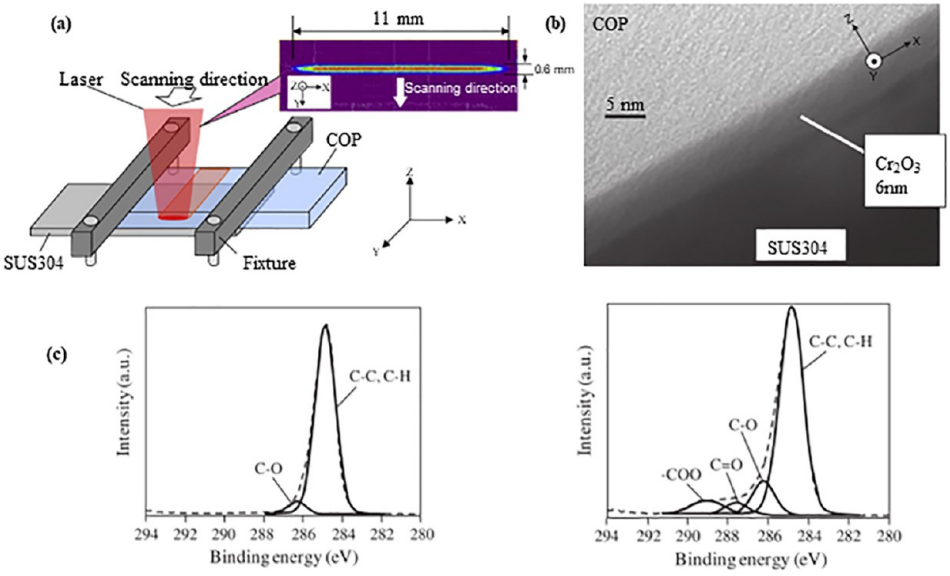

Figure 8. (a) Schematic diagram of laser joining, (b) TEM image of the interface between COP and SU304, and (c) C 1s spectra of COP, reproduced with permission from Arai et al. Copyright 2014, Elsevier Ltd.[59]

shows that C−O and C═O increase and newly generate COO bonds on the COP surface. The percentage of oxygen functional groups and the surface binding energy significantly increased, indicating that the improved mobility of oxygen functional groups with COP improves the strength of the connection.

3.2. Short-Fiber-Reinforced Resin. The short-fiber-reinforced composites with random orientation are less expensive to create, easier to automate, and more moldable than continuous long-fiber composites.[60] Short-fiber-reinforced thermoplastic composites have high mechanical qualities due to their high short-fiber content.[61,62] With the benefit of short fibers, the resin is reinforced with short fibers, which can improve the adhesion between stainless steel and resin. Cui et al.[63] performed the resistance welding with SSM after using carbon fiber-reinforced PEI resin, and the experimental procedure is shown in Figure 9a. Figure 9b shows the SEM image of the PEI film, in which it can concluded that the surface of the pure PEI film is smoother, and the internal and surface fibers of the fiber-reinforced PEI composite film are disordered. Figure 9c shows that the tensile strength of the fiber-reinforced PEI film is significantly higher, compared to the pure PEI film. Figure 9d shows that the welded joint strength of the fiber-reinforced is higher than that of the welded joint without the addition of fibers.

Zhao[35] found that the addition of fibers to the weld head in the stainless steel mesh and the weld body of the interlayer failure changed. By transforming to stainless steel mesh and fiber tearing, the mechanical properties of the welded head were significantly improved. Wang et al.[52] found that short Kevlar fibers (SKF)-reinforced epoxy resin improved the shear strength between the steel plate and stainless steel. SKF reinforcement has a better shear strength because the cohesion damage to multiwall carbon nanotube reinforcement is primarily in the bonding. Shi et al.[64] found that SCF was distributed in PE after short-carbon fiber-reinforced PE resin. The load of the hybrid welding interface was taken up, which improved the shear strength of the welded joint.

3.3. Resin Modification. The interface contact between the resin and stainless steel can be significantly improved by

https://doi.org/10.1021/acsomega.3c05728
ACS Omega 2023, 8, 39984−40004

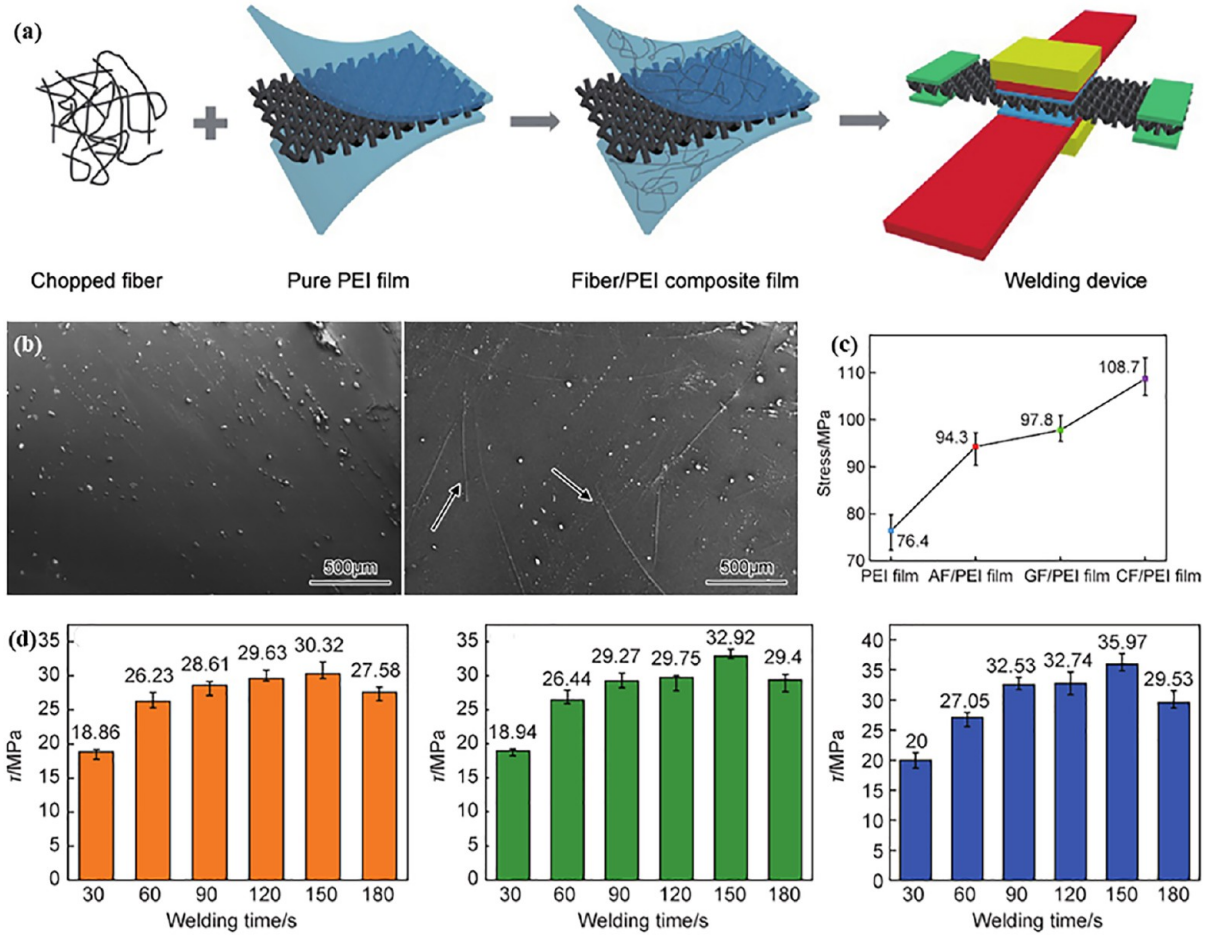

Figure 9. (a) Schematic diagram of the welding, (b) SEM images of film, (c) tensile strength of film, and (d) fiber-reinforced resin composite film for enhancing the strength of the welded interface. Image courtesy of Cui et al.[63]

adding chemical groups to the resin through chemical reaction. In recent years, epoxy-modified silicone resins have received widespread attention, and their applications have been continuously expanded..[65] Zou et al.[66] introduced polar functional groups into the nonpolar chain of polypropylene through grafting reaction and subjected the stainless steel mesh in GF/PP/SSM laminates to surface decay and phosphorus treatment, thereby improving the bonding strength between metal and stainless steel. Zhang et al.[67] designed poly[glycidyl methacrylate-*co*-(*N*-(3,4-dihydroxyphenethyl)methacrylamide] [P(GMA-*co*-DOMAm)] shown in Figure 10a. The catechol unit acts as an anchoring group, and the epoxy group enables the epoxy−amine reaction to improve the interaction between the metal surface and the epoxy binder. Figure 10b shows that after 60 min of polymer adsorption, the C/O ratio was as high as 1.01. Figure 10c shows the uniform adsorption of the polymer on the SUS surface and the completion of the P(GMA-*co*-DOMAm) adsorption. The specimens were subjected to pull-off testing. The microscope image in Figure 10d shows that the adhesive appeared on only one SUS plate. It indicates that the adhesion is enhanced after polymer treatment.

In addition to the epoxy resin that has been chemically changed, UV treatment can impart new chemical groups to the resin to increase its adherence to stainless steel. UV treatments are usually prolonged as the result of chemical changes on the surface. Scarselli et al.[68] found the UV treatment process produced carbonyl groups that produced a strong chemical bond with the epoxy resin binder.

4. ADHESION TEST METHOD OF STAINLESS STEEL AND RESIN

The interfacial bonding qualities of stainless steel and resin can be evaluated using macroscopic and microscopic mechanical testing methods. Microscopic tests use monofilament pull-out, while macroscopic tests use fracture toughness and interlaminar shear strength tests. The published research on adhesion testing techniques is summarized in Table 3.

4.1. Monofilament Pull-out. There are five testing procedures for determining the interfacial bonding characteristics of composites that are widely used. Depending on the applied stress or object, they include the following: monofilament pull-out, microbond, monofilament extrusion, monofilament fragmentation, and Broutman. The experiments using the microbond method are a sophisticated way of examining the interfacial strength of the composites. Nishikawa et al.[69] measured the fracture toughness of fiber-reinforced composite interfaces by pulling the fibers out of the droplets of the matrix through a knife edge. Microbond tests were performed by T800S carbon fiber specimens with epoxy droplets. The scanning electron microscope (SEM) was able to observe the droplets on the fibers, the location of the tracts, and the matrix cracking in the meniscus area. According to the fiber breaking strain and Hooke's law, it is known that the pull-out force is at

https://doi.org/10.1021/acsomega.3c05728
ACS Omega 2023, 8, 39984−40004

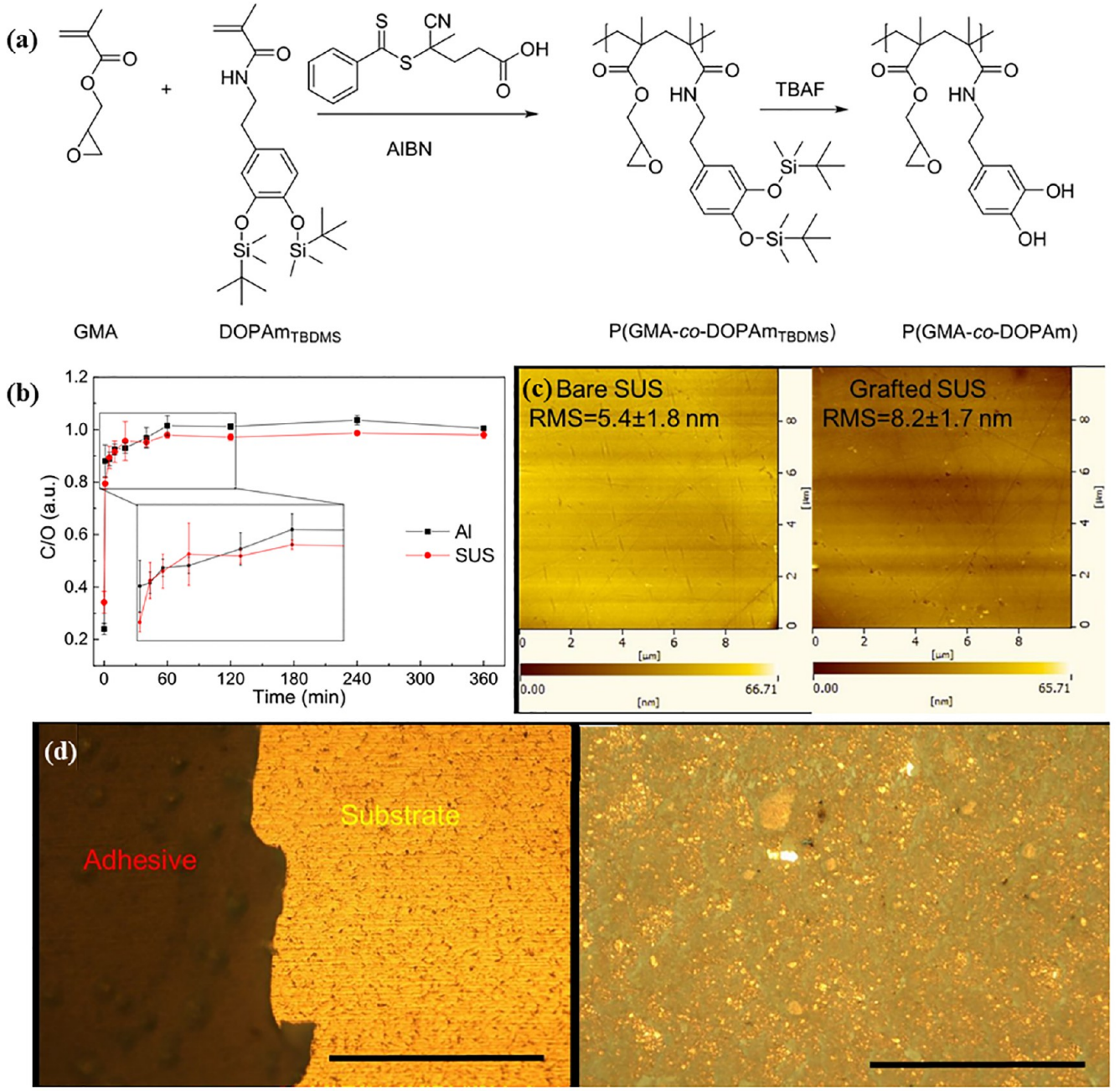

Figure 10. (a) Synthesis strategy of P(GMA-*co*-DOPAm), (b) C/O ratio of SUS (red line) and Al (black line) plates with various immersion durations, (c) surface morphology of SUS sample, and (d) microscope observation of the adhesion area in SUS joints; image courtesy of Zhang et al.[67]

most 0.12 N. Li et al.[26] prepared a microbond test sample of the monofilament SS wire and the polymer matrix on a U-shaped metal plate, as shown in Figure 11a. Microbond tests were performed to determine the IFSS of the SS wire and the polymer matrix. Figure 11b shows the fracture morphology of the PPEK droplets on the SS wire. The surface morphology of the untreated SS wire was smooth, and the PEEK droplet was successfully peeled off from the SS wire. The treated SS wire was severely damaged in the contact area with the PEEK. By IFSS testing, the results are shown in Figure 11c, and the IFSS increased from 28 to 34 MPa.

Microbond and monofilament extraction methods are probably the most popular due to the their ease of experimental design, the ability to utilize well-defined test geometries, and the excellent reproducibility of their results. It is simple to define the interfacial bonding characteristics of stainless steel to the resin matrix. The monofilament pull-out method differs from other micromechanical tests in that it applies to most softer and rigid fibers and ductile and brittle substrates. These substrates can be either thermoplastic or thermosetting. The monofilament pull-out technique involves burying the monofilament vertically in the matrix and removing it after curing and measuring the tensile force needed to extract the fibers to determine the flexural strength.[70] The usage of the method is constrained by the length of the fibers buried in the matrix. If the fibers are too long, they are likely to shatter during extraction. Zhao[35] pulled the stainless steel wire out of the PEI resin drops by a knife tip.

https://doi.org/10.1021/acsomega.3c05728
ACS Omega 2023, 8, 39984−40004

Table 3. Adhesion Test Methods

test method	standard	specimen	test characteristic	conclusion	ref
microbond method		T800CF/epoxy−resin	IFSS	Pull-out force of up to 0.12 N was obtained.	69
	ASTM-D1002	SSwire/PEEK	IFSS	IFSS increased from 28 to 34 MPa.	26
monofilament pull-out		GF/PEI	IFSS	IFSS value between stainless steel wire and PEI resin increased from 2.76 to 7.98 MPa.	35
single-lap test	ASTM D5868-01(2014)	steel plate/CFRP	LSS	The shear strength was 7.78 MPa/mm at −25 °C and 2.52 MPa/mm at 100 °C, a decrease of 67.6%.	71
	ASTM D3165-07, ASTM D3762	SS/epoxy−resin	LSS	When stainless steel was activated by He/O_2 plasma, the lap shear strength increased by 33.1 MPa.	49
	ASTM D3164M-98	polyethylene/graphene flakes composites	LSS	When the GFs concentration was 0.5 wt %, the shear strength reached the maximum value of 9.42 MPa.	72
	ASTM D1002	CF/PEEK	LSS	CF/PEEK joints treated with silane coupling agents on stainless steel surfaces increased to 40 MPa, an increase of 9%.	26
double-lap test		steel plate/CFRP	LSS	When the temperature was higher than 70 °C, CFRP plates were torn.	73
		TC350−1/IM7-12K, 5528A/CCF300	LSS	Structural shear strength decreased by 22.9% after moist heat.	74
	ASTM D3528	CF/PEI, GF/PEI, CF/PEEK, CF/PEKK	LSS	F/PEI and GF/PEI specimens exhibited linear behavior until maximum load followed by abrupt damage, while CF/PEEK and CF/PEKK specimens exhibited linear behavior initially followed by a nonlinear response to damage	75
pull-off test	ASTM D2095-96	polyethylene/graphene flakes composites		It is concluded that when the GFs concentration was 0.5 wt %, the tensile adhesion strength reached the maximum value of 4.23 MPa.	72
	ISO 4624:2003	SS/epoxy−resin		The highest surface finish had a frame strength of over 60 MPa.	25
mode I fracture toughness	ASTM D5528-01	CF/steel composite structure	DCB	The mode I fracture energy of the bonding interface of the sandblasted/MWCNT specimen was greater than those of the other three interfaces.	73
	-	CF/polymer matrix composites	WDCB	The average fracture toughness obtained from J-integral fracture toughness was 0.36 N/mm.	81
mode II fracture toughness	-	CF/steel composite structure	ENF	The fracture energy and the final slip distance of the interviewed parts of the grooved/Kevlar/MWCNT bonding interface were greater than those of the other two interfaces.	82
	ESIS protocol	flax/basalt-reinforced vinyl ester hybrid composites	3ENF	The fracture energy of FBVEu composites, G IIC init., and G IIC prop. were increased by 58% and 21%, respectively, compared to that of FVE dry specimens.	83
	ASTM D7905	CF/thermoplastic liquid acrylic resin	ENF	Compared to conventional epoxy-based carbon fiber composites, thermoplastic laminates exhibited higher resistance to crack expansion.	84
	ASTM 7905	GRFP	ENF	The delamination growth of NPC specimens was unstable, and the final value of the average GIIC was 2.08 N/mm.	85
mode III fracture toughness		glass/epoxy steel dual material	ECT	The mode III fracture toughness values were lower for both materials, with an average value of about 80%.	86
		carbon/epoxy tape	ECT	Stratification toughness of the ECT test was related to insertion length.	87
		AS4/8552, AS4/35011-6, IM7/MT M45-1	LHFB	The LHFB device can effectively obtain static and cyclic fatigue ERR values for laminated composites regardless of the mode of resin that made up their matrix.	88

https://doi.org/10.1021/acsomega.3c05728
ACS Omega 2023, 8, 39984−40004

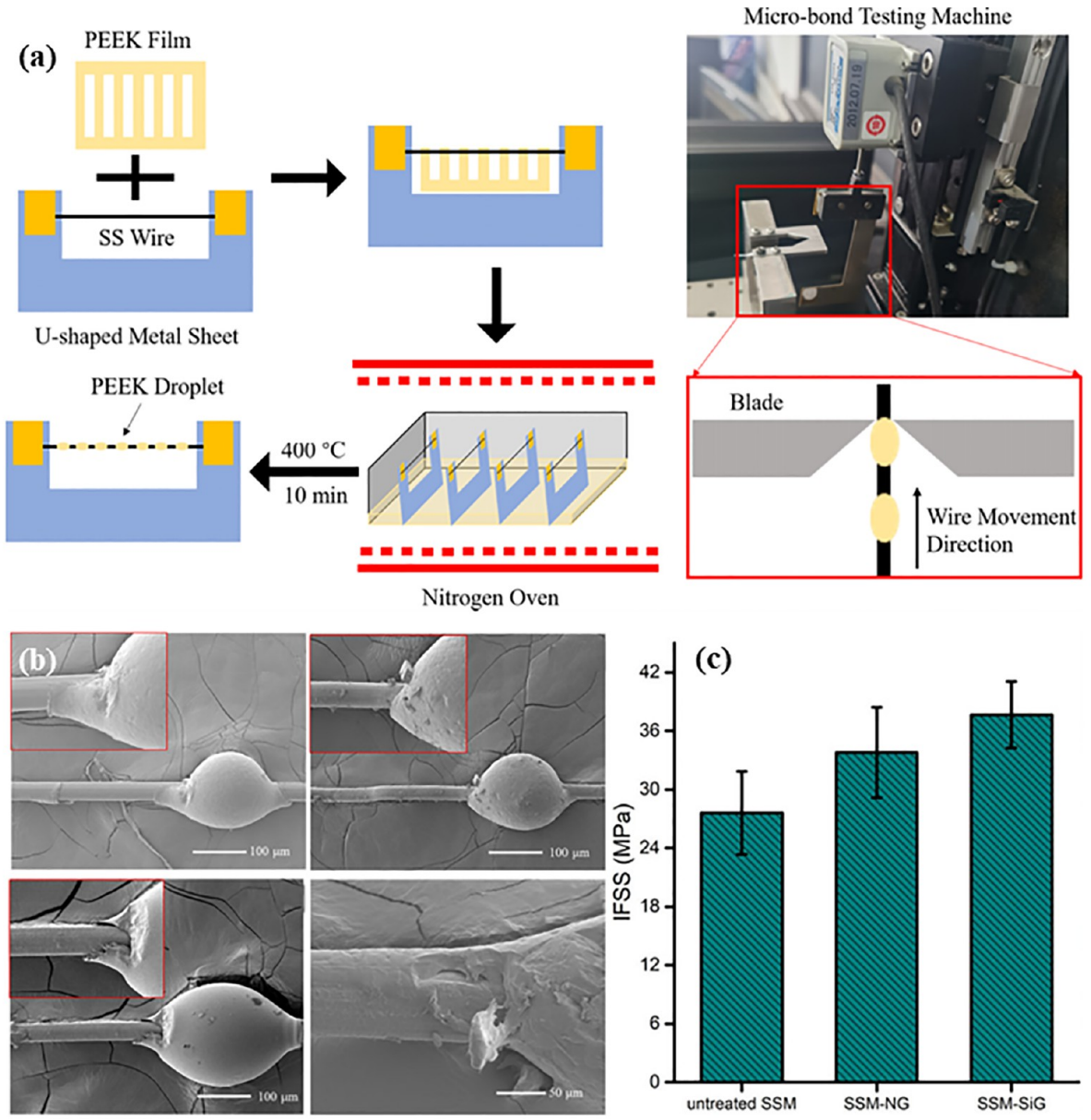

Figure 11. (a) Schematic illustration of the preparation of microbond test samples, (b) fracture morphology of PEEK droplets on the SS wires, and (c) IFSS results. Image courtesy of Li et al.[26]

The test results show that the IFSS value between the stainless steel wire and PEI resin increased from 2.76 to 7.98 MPa after grafting CNT. Chen et al.[40] measured the adhesion between the test piece and the epoxy-based resin by pull-off testing and inserting the test piece into the resin. Through the test results, they concluded that the adhesion between the plasma jet-treated stainless steel and the epoxy-based resin was improved.

The IFSS testing of the composite materials is challenging due to the many variables influencing the results. In addition, since the research object in the sample making and testing phases is single filament, it leads to strict requirements for operation. Even the smallest mistake can easily result in a broken filament.

4.2. Lap Test. The size of the lap shear strength can reflect the solid degree of stainless steel and resin bonding; the stronger the bond, the better the process performance. It is often used to evaluate the welding quality of the macro-composites. It is divided into single-lap test and double-lap test according to the form of the joint. A single -lap joint will bend under a tensile load because the loading surface and the symmetry of the connection are not coplanar; however, a double-lap joint can reduce the bending force and deformation.

4.2.1. Single-Lap Test. Zhu et al.[71] conducted single-lap tests on the steel plates and the CFRP with reference to ASTM D5868-01 (2014). Williams et al.[49] performed single-lap shear tests with reference to ASTM D3165-07 and ASTM D3762, and the plasma treatment resulted in maximum shear strength. Chen et al.[50] studied the influence of different parameters of the adhesive layer and structure on the connection performance of laminates and studied the shear strength through single-lap experiments, according to GB/T 3334-2016. Liu et al.[66] performed single-lap shear tests on polyethylene/graphene sheet composites with stainless steel according to ASTM D3164M-98. Shear strength reaches the maximum value of 9.42 MPa when the GFs concentration is 0.5 wt %.

https://doi.org/10.1021/acsomega.3c05728
ACS Omega 2023, 8, 39984−40004

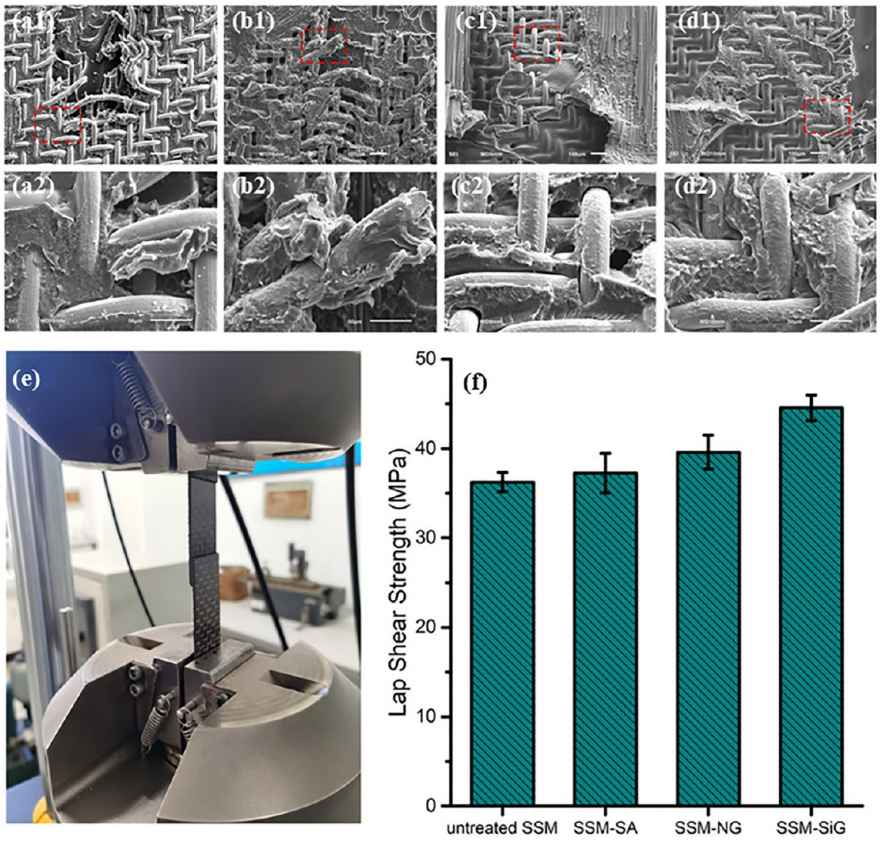

Figure 12. Fracture surfaces of welded joints after lap shear tests for (a1), (a2) untreated SSM; (b1), (b2) SSM-SA; (c1), (c2) SSM-NG, and (d1), (d2) SSM-SiG; (e) LSS testing; (f) LSS of untreated SSM, SSM-SA, SSM-NG, and SSM-SiG welded joints, image courtesy of Li.[26]

Li et al.[26] performed LSS tests at room temperature as shown in Figure 12e. Figure 12f shows that the increase in CF/PEEK joints after silane coupling agent treatment of the stainless steel surface to 40 MPa is 9%. Figure 12a1−d2 shows SEM images of the fracture surface, and the gap between SSM-SiG (silane coupling agent treated) is covered by PEEK with a high residual resin content on the surface, showing good adhesion between SSM-SiG.

4.2.2. Double-Lap Test. Chen et al.[73] investigated the effect of different temperatures on double-lap joints of the steel CFRP sheets by double-lap joints. Gao et al.[74] tested the shear strength of the composite double-lap specimens in a damp heat environment according to ASTM D638, and they concluded that the shear strength of the structure decreased by 22.9% after damp heat. Dubé et al.[75] investigated resistance welding of the thermoplastic composite double-lap joints with the operation schematic shown in Figure 13a. The sample strip with dimensions of 190.5 mm in length and 25.4 mm in width was generated using the ASTM D3528 test procedure. The lap shear test was performed using the experimental setup in Figure 13b. The load−displacement curve of the double-lap shear specimen was obtained as shown in Figure 13c. The CF/PEI and GF/PEI specimens showed linear behavior until maximum load followed by abrupt damage. The CF/PEEK and CF/PEKK specimens showed linear behavior initially followed by a nonlinear response to damage. By observing the fracture of the CF/PEKK examples during fatigue loading, it is possible to identify different regions where the fibers and polymer exhibit good adhesion. The IFSS test data can reflect the actual interfacial bonding state of stainless steel and resin matrix. Therefore, IFSS is the most used test method to characterize the interfacial bonding strength of composite materials in industrial production.

4.3. Pull-off Test. The bonding force of the composite and stainless steel can be evaluated using a pull-off test. The specimen geometry and dimensions are presented in Figure 14a. Liu et al.[72] performed adhesive bond tension tests on polyethylene/graphene sheet composites according to the ASTM D2095-96 standard, and the specimen geometry and dimensions are shown in Figure 14a. They concluded that when the GFs concentration was 0.5 wt %, the tensile bond strength reached a maximum value of 4.23 MPa, as shown in Figure 14b. Ghosh et al.[25] performed pull-off tests according to the ISO 4624:2003 standard, using the sample preparation scheme and test method. The surface-treated SS plate inserted between the carts and the glass beads controls the thickness of the epoxy resin layer. After the epoxy resin cured, a pull-off test was performed with a speed setting of 0.5 mm/min.

4.4. Fracture Toughness. Fracture toughness is a quantitative indicator of the ability of a material to prevent crack expansion and a measure of the toughness of a material. Fracture toughness refers to the measure of the ability of a material to prevent the expansion of macroscopic crack instability and a toughness parameter of a material to resist brittle damage. Different stress states of the same material in the same environment will lead to different deformations and crack states. In fracture mechanics, the fracture mode of cracks is usually divided into three models,[76] as illustrated in Figure 15.[77] Among them, mode I cracks belong to the open mode cracks, and the member I is mainly subjected to tensile load

https://doi.org/10.1021/acsomega.3c05728
ACS Omega 2023, 8, 39984−40004

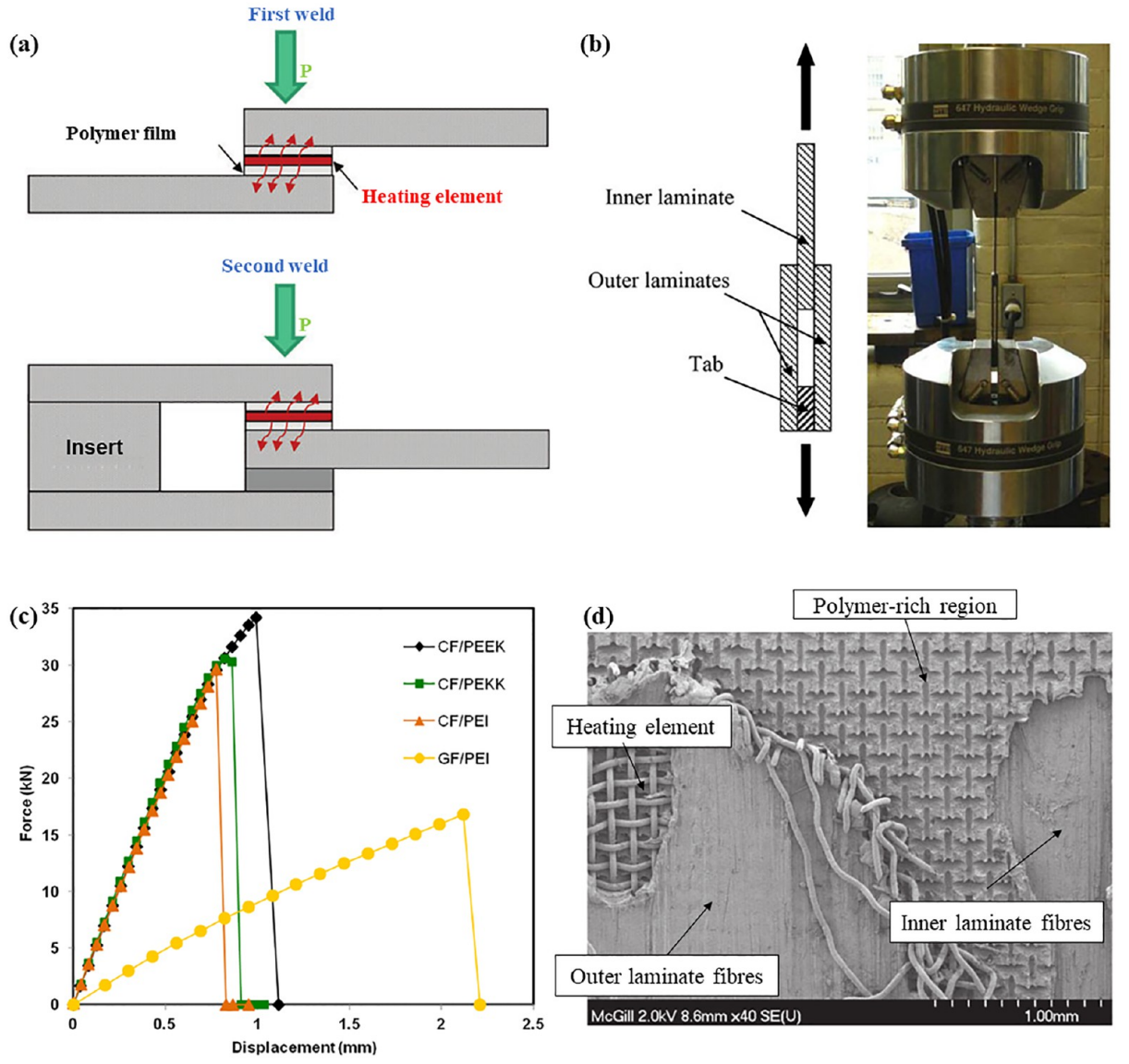

Figure 13. (a) Schematic representation of resistance welding operations for double-lap shear joints, (b) schematic representation of a DLS specimen and picture of the test setup, (c) load−displacement curves of double-lap shear specimens, and (d) typical fracture surface of CF/PEKK DLS specimens tested under fatigue loading. Image courtesy of Dubé.[75]

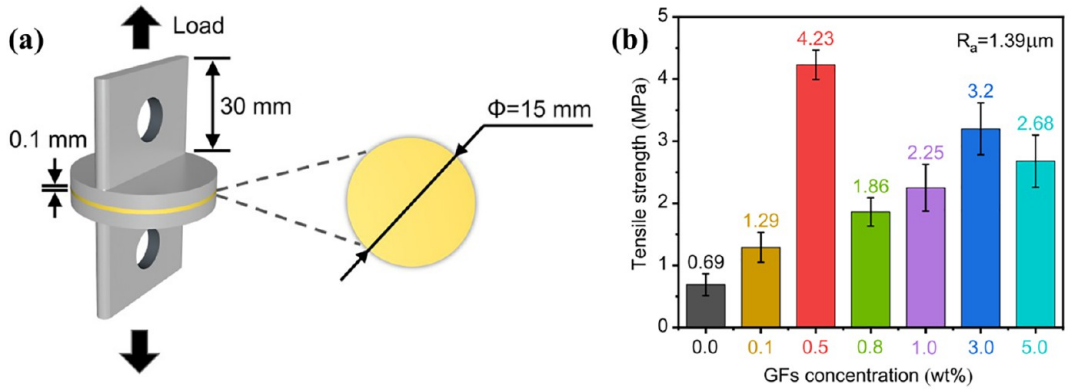

Figure 14. (a) Diagram of the adhesive tensile specimen, (b) tensile adhesive strength with respect to GFs concentrations, reproduced with permission from Liu et al. Copyright 2021, Elsevier Ltd.[72]

https://doi.org/10.1021/acsomega.3c05728
ACS Omega 2023, 8, 39984−40004

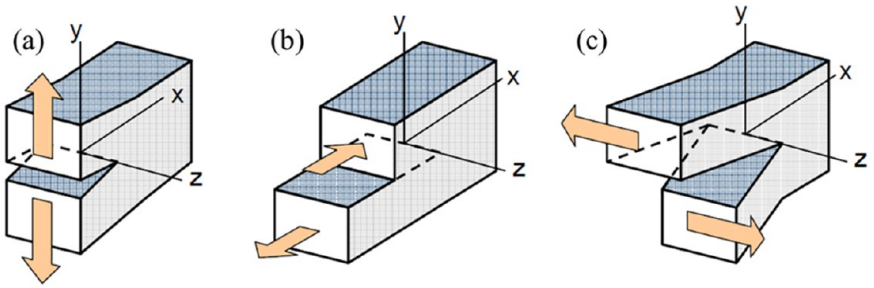

Figure 15. Three modes of fracture: (a) mode I crack extension; (b) mode II crack extension; (c) mode III crack extension. Image courtesy of Wang.[77]

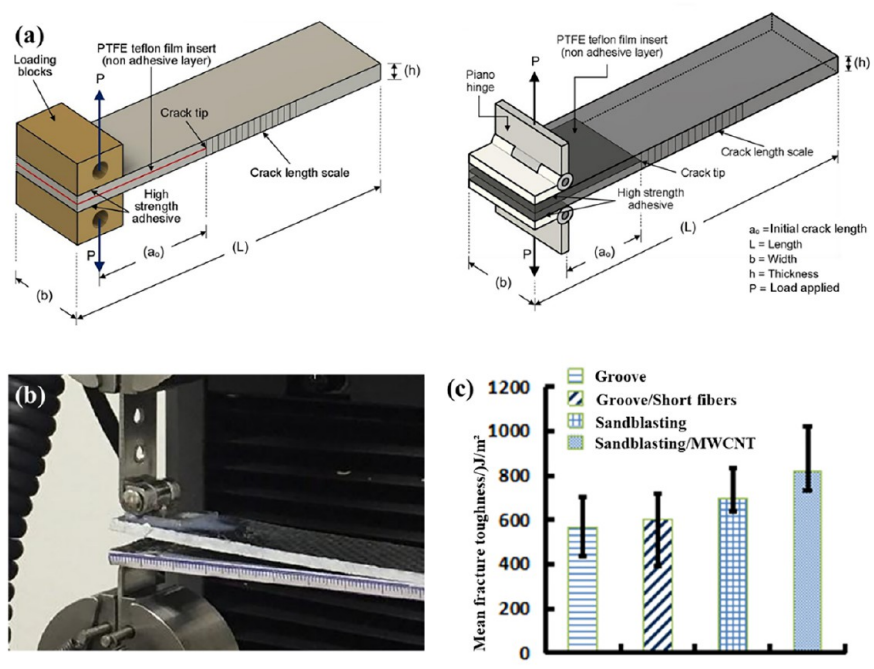

Figure 16. (a) Mode I interlaminar fracture toughness test setup (DCB specimen with loading blocks and with piano hinges), reproduced with permission form Sharma et al. Copyright 2020 Iran Polymer and Petrochemical Institute;[80] (b) DCB experimental process diagram; (c) mean fracture toughness. Image courtesy of Wang.[77]

perpendicular to the crack direction.[78] Mode II cracks belong to the slip-mode cracks, and the member is mainly subjected to shear load parallel to the crack direction. Mode III crack is a tearing crack, and the member is mainly subjected to shear load parallel to the crack surface and perpendicular to the crack direction.[77] Currently, the commonly used fracture toughness specimens are three-point bending specimens and compact tensile specimens. The test method is to open a crack in the middle of the specimen, through the three-point or four-point bending fracture test, to get the material fracture toughness. Chandrasekaran et al.[79] used the Zwick Roell Z010 universal testing machine to evaluate fracture toughness using a three-point end-notch bending test.

4.4.1. Mode I Fracture Toughness. Mode I cracks expand mainly at the connecting interfaces among the bonding layer and the carbon fiber laminate, the bonding layer and the steel plate surface, and the bonding layer itself when a carbon fiber/steel composite structure is damaged. The double cantilever beam method (DCB), which is frequently employed in composite laminate mode I fracture toughness test locations, is depicted in Figure 16a.[80] Wang[77] used DCB to conduct testing on four bonding interfaces (immediate groove, grooved/short fiber, sandblasted, and sandblasted/MWCNT) specimens in line with the ASTM D5528-01 standard, as shown in Figure 16b. Figure 16c shows the average fracture toughness graph, and the mode I fracture energy of the bonding interface of the sandblasted/MWCNT specimen is larger than the other three interfaces. Ding and Xu[81] tested the composite by a wedge-embedded double cantilever beam (WDCB), to apply and verify the J-integral to determine mode I fracture toughness under large deformation. Experiment results were obtained for the J-integral of the mode I fracture toughness of the composite WDCB and a simplified method for the available data. It was feasible to calculate the correct power extraction efficiency of WDCB using the J-integral.

4.4.2. Mode II Fracture Toughness. The relative displacement directions of the upper and lower surfaces of a mode II slip-mode crack are distinct, with one cracking surface moving in the same direction as the crack expansion and the other cracking surface moving in the opposite direction. The test methods for mode II fracture toughness of composite materials are confined layer slip (CLS), end load split (ELS), and end-

https://doi.org/10.1021/acsomega.3c05728
ACS Omega 2023, 8, 39984−40004

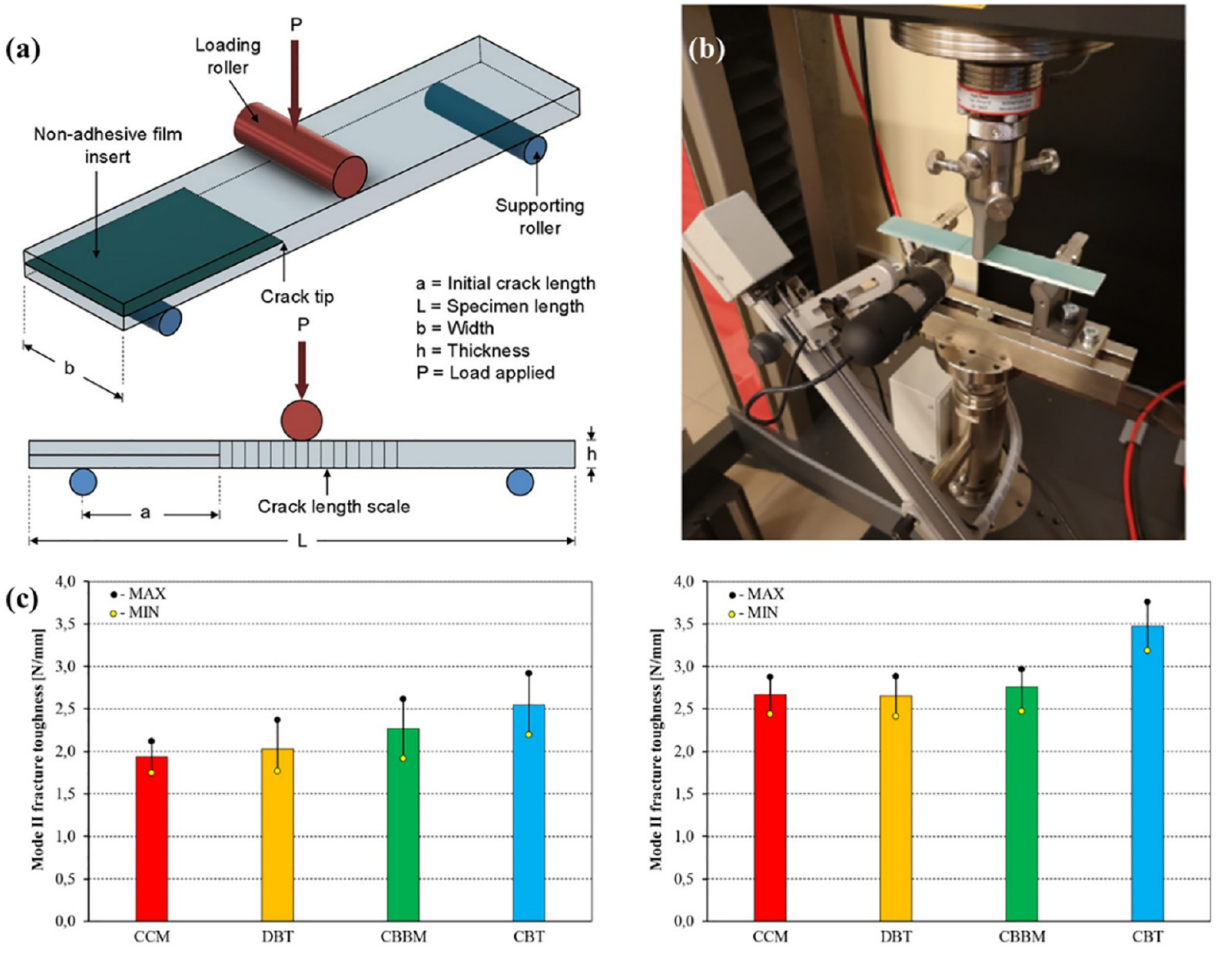

Figure 17. (a) Mode II interlaminar fracture toughness test setup (ENF specimen), reproduced with permission form Sharma et al. Copyright 2020, Iran Polymer and Petrochemical Institute.[80] (b) ENF test fixture and (c) mode II fracture toughnesses obtained for considered GFRP laminate by using different data reduction schemes for PC and NPC specimens; image courtesy of Gliszczynski and Wiącek.[85]

notched flexure (ENF), etc. The ENF test method has become the most commonly used test method because of its advantages of easy processing of the specimen and simplicity of the test. The test setup and specimen are shown in Figure 17a. Luo[82] tested specimens for three bonding interfaces (instant groove/Kevlar, grooved/Kevlar/MWCNT, and sand-blasted/MWCNT). The test results show that the fracture energy and final slip distance of the specimens interviewed at the grooved/Kevlar/MWCNT bonding interface are greater than those of the other two interfaces.

Almansour et al.[83] tested the flax/basalt-reinforced vinyl ester composites by the three-point end-notch bending (3ENF) test to measure the crack length and critical strain energy release rate G_{IIC}. The mode II fracture toughness of flax/basalt-reinforced vinyl ester composites was obtained by testing. Barbosa et al.[84] conducted mode II fracture toughness tests on epoxy composites with reference to the ASTM D7905 M 14 test standard. Gliszczynski and Wiącek[85] performed end-notch flexure (ENF) tests on GRFP unidirectional laminates, with specimens manufactured according to ASTM 7905. The initial length of precracking was 30 mm, and the experimental procedure fixture is shown in Figure 17b. The end value of the average G_{IIC} was 2.08 N/mm, indicating that the delamination development of the NPC specimens was unstable.

4.4.3. Mode III Fracture Toughness. Mode III fracture toughness is also known as fracture tear mode, and there are test methods for mode III fracture toughness of composite materials, such as Split Cantilever Beam (SCB), Edge Ring Crack Torsion (ERCT), and Longitudinal Half Fixed Beam (LHFB). It is mainly characterized by edge crack torsion (ECT) test specimens with specimen size and external loading system.[80] Pennas and Cantwell[86] investigated the mode III fracture toughness of a glass/epoxy steel bimaterial system using ECT test geometries. Audd et al.[87] conducted edge crack torsion tests on laminated composites, with ECT specimens prepregged with carbon/epoxy tape.

The characterization of composites in mode III fracture mode is equally applicable to the longitudinal semifixed beam (LHFB) test. Bertorello et al.[88] performed LHFB tests on three different modes of composites: Hexply AS/8552 RC34 AW196 (8552), Hexply AS/3501-6 RC37 AW190 (3501-6), and ACG MTM45-1/IM7-145 (MTM45-1), using the experimental setup as shown in Figure 18a. The experimental results obtained are shown in Figure 18b, where the fatigue performance loss of the AS4/35011-6 material during fatigue is low. Figure 18c shows the micrographs of different materials, and the AS4/8552 material demonstrates fracture fibers and a typical mode III fracture. The AS4/3501-6 material shows a sawtooth-dominated morphology with few fractured fibers.

https://doi.org/10.1021/acsomega.3c05728
ACS Omega 2023, 8, 39984−40004

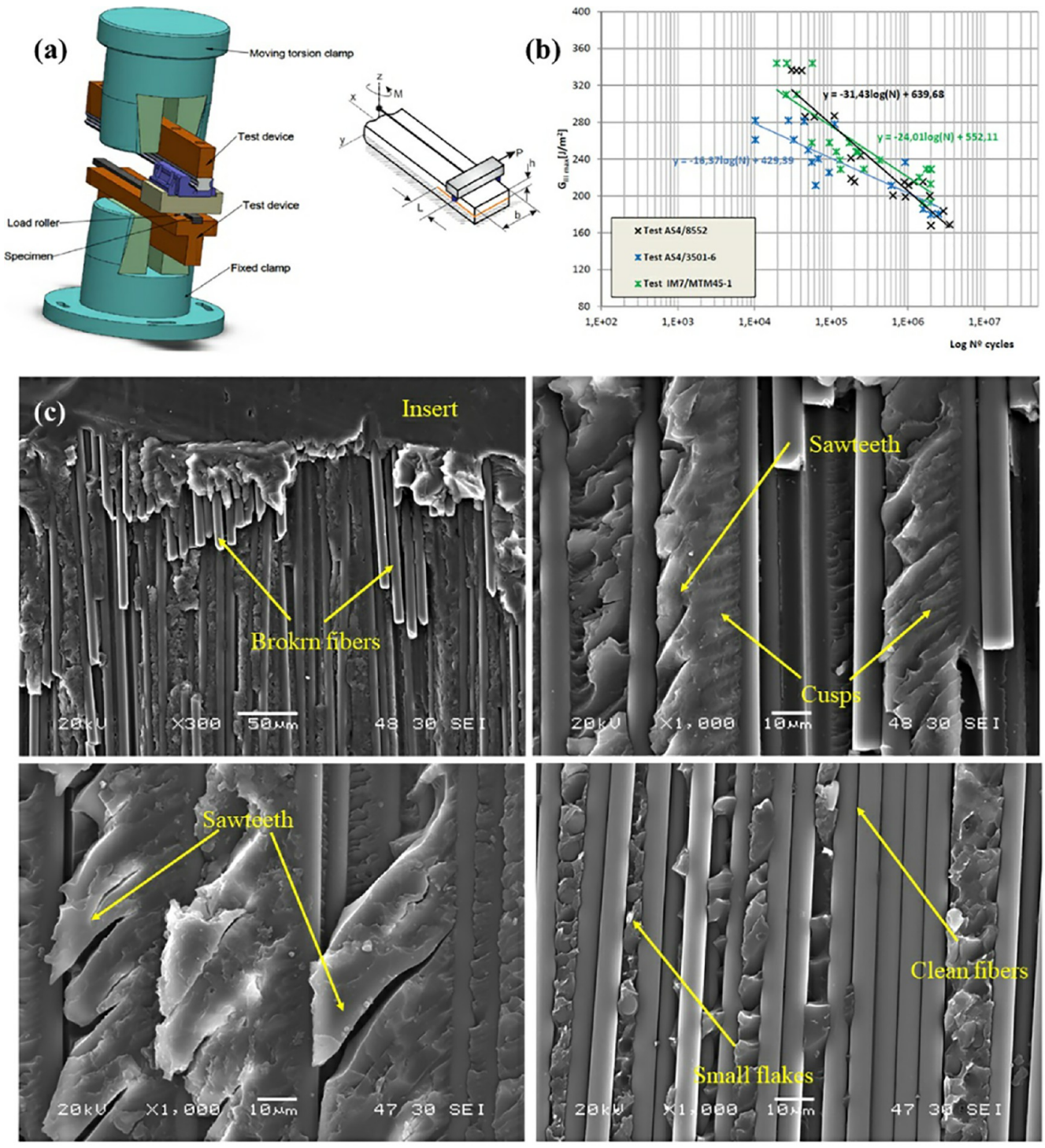

Figure 18. (a) Mode III fracture test device, (b) results of all tests performed for all three materials at different percentages of the maximum torque, and (c) micrographs of different materials. Image courtesy of Bertorello et al.[88]

The fractured picture of the IM7/MT M45-1 material shows almost no fractured fibers. The findings demonstrate that laminated composites can efficiently obtain static and cyclic fatigue ERR values using the LHFB device without taking the mode of resin that makes up their matrix into account.

5. CONCLUSIONS AND PROSPECTS

In summary, the main methods to improve the adhesion of stainless steel and resin interface are stainless steel surface silane coupling agent treatment, oxidation treatment, chemical etching, plasma treatment, carbon nanotubes (CNTs) treatment and resin CNTs reinforcement, fiber reinforcement, and chemical modification. Among them, stainless steel surface silane coupling agent treatment, oxidation treatment, chemical etching, and plasma treatment can effectively improve the surface roughness of stainless steel and increase the oxygen-containing polar functional groups. It is beneficial to promote the formation of mechanical interlocking and chemical

https://doi.org/10.1021/acsomega.3c05728
ACS Omega 2023, 8, 39984−40004

bonding between stainless steel and resin matrix, thus improving the interfacial properties of stainless steel and resin. Microscopic level monofilament pull-out and macroscopic level fracture toughness and interlaminar shear strength tests are mainly used to characterize the interfacial bond strength. Future attempts to improve the adhesion between stainless steel and resin interfaces are as follows:

(1) Most of the researchers' methods for improving the adhesion of stainless steel and resin are for stainless steel or resin alone. In the future, the integrated combination of stainless steel surface treatment and resin modification can be further explored.

(2) For the chemical etching, interfacial characterization at the microscopic level allows for more adequate regulation of the interfacial microstructure and better interfacial bonding properties.

(3) The introduction of CNTs in both stainless steel and resin can improve the interlayer properties to some extent, but there are some problems influenced by the method of CNT introduction. How to realize the uniform dispersion more simply and effectively of carbon nanotubes is a direction worthy of future research.

(4) In the future, the effect of more environmental factors such as the heat resistance, corrosion resistance, and aging resistance of stainless steel and resin interface can be explored.

■ ASSOCIATED CONTENT

Data Availability Statement

The data sets generated during and/or analyzed during the current study are available from the corresponding author on reasonable request.

■ AUTHOR INFORMATION

Corresponding Authors

Bing Du − *Chongqing Key Laboratory of Nano−Micro Composite Materials and Devices, School of Metallurgy and Materials Engineering, Chongqing University of Science and Technology, Chongqing 401331, China; College of Aerospace Engineering, Chongqing University, Chongqing 400030, China*; orcid.org/0000-0003-4178-9434; Email: dubing@cqust.edu.cn

Hanjie Hu − *School of Aeronautics, Chongqing Jiaotong University, Chongqing 400074, China; The Green Aerotechnics Research Institute of CQJTU, Chongqing 401120, China*; Email: huhj@gatri.cn

Authors

Xinyu Zhou − *Chongqing Key Laboratory of Nano−Micro Composite Materials and Devices, School of Metallurgy and Materials Engineering, Chongqing University of Science and Technology, Chongqing 401331, China*

Qichang Li − *Chongqing Key Laboratory of Nano−Micro Composite Materials and Devices, School of Metallurgy and Materials Engineering, Chongqing University of Science and Technology, Chongqing 401331, China*

Jingwei Liu − *Chongqing Key Laboratory of Nano−Micro Composite Materials and Devices, School of Metallurgy and Materials Engineering, Chongqing University of Science and Technology, Chongqing 401331, China*

Yuxi Liu − *School of Smart Health, Chongqing College of Electronic Engineering, Chongqing 401331, China*

Xianjun Zeng − *The Green Aerotechnics Research Institute of CQJTU, Chongqing 401120, China*

Xiangrong Cheng − *Chongqing Key Laboratory of Nano−Micro Composite Materials and Devices, School of Metallurgy and Materials Engineering, Chongqing University of Science and Technology, Chongqing 401331, China*

Complete contact information is available at: https://pubs.acs.org/10.1021/acsomega.3c05728

Notes

The authors declare no competing financial interest.

■ ACKNOWLEDGMENTS

This research was funded by National Natural Science Foundation of China (12202088), Chongqing Natural Science Foundation (CSTB2022NSCQ-JQX0024), Chongqing Postdoctoral Research Project (2022CQBSHTB2023), Science and Technology Research Program of Chongqing Municipal Education Commission (KJQN202101531), and Fundamental Research Funds for the Central Universities (2022CDJQY-004).

■ REFERENCES

(1) Jin, Z.; Han, Z.; Chang, C.; et al. Review of methods for enhancing interlaminar mechanical properties of fiber-reinforced thermoplastic composites: Interfacial modification, nano-filling and forming technology. *Compos. Sci. Technol.* **2022**, *228*, 109660.

(2) Rajak, D. K.; Pagar, D. D.; Menezes, P. L.; et al. Fiber-reinforced polymer composites: Manufacturing, properties, and applications. *Polymers* **2019**, *11* (10), 1667.

(3) Yao, S. S.; Jin, F. L.; Rhee, K. Y.; et al. Recent advances in carbon-fiber-reinforced thermoplastic composites: A review. *Composites Part B: Engineering* **2018**, *142*, 241−250.

(4) Khan, R. Fiber bridging in composite laminates: A literature review. *Composite Structures* **2019**, *229*, No. 111418.

(5) Zhang, J.; Chevali, V. S.; Wang, H.; et al. Current status of carbon fibre and carbon fibre composites recycling. *Composites Part B: Engineering* **2020**, *193*, No. 108053.

(6) Forintos, N.; Czigany, T. Multifunctional application of carbon fiber reinforced polymer composites: Electrical properties of the reinforcing carbon fibers−A short review. *Composites Part B: Engineering* **2019**, *162*, 331−343.

(7) Du, B.; Li, Q. C.; Zheng, C. Q.; et al. Application of lightweight structure in automobile bumper beam: a review. *Materials* **2023**, *16* (3), 967.

(8) Ahmad, H.; Markina, A. A.; Porotnikov, M. V.; et al. A review of carbon fiber materials in automotive industry[C]//IOP Conference Series: Materials Science and Engineering. *IOP Publishing* **2020**, *971* (3), No. 032011.

(9) Dawei, Z.; Qi, Z.; Xiaoguang, F.; et al. Review on joining process of carbon fiber-reinforced polymer and metal: Applications and outlook. *Rare Metal Mater. Eng.* **2019**, *48*, 44−54.

(10) Budhe, S.; Banea, M. D.; De Barros, S.; et al. An updated review of adhesively bonded joints in composite materials. *Int. J. Adhes. Adhes.* **2017**, *72*, 30−42.

(11) Zhao, J.; Chu, L.; Liu, J.; et al. Effect of micro-arc oxidation treatment on adhesion properties between stainless steel and epoxy resin. *Heat Treatment of Metals* **2020**, *45* (03), 92−97.

(12) Li, N.; Wang, G. d.; Melly, S. K.; Peng, T.; Li, Y. C.; Di Zhao, Q.; de Ji, S.; et al. Interlaminar properties of GFRP laminates toughened by CNTs buckypaper interlayer. *Composite Struct.* **2019**, *208*, 13−22.

(13) Li, J.; Huang, Y.; Xu, Z.; et al. High-energy radiation technique treat on the surface of carbon fiber. *Mater. Chem. Phys.* **2005**, *94* (2−3), 315−321.

(14) Wang, T.; Gao, C.; Xu, H. Research progress on interface mechanical property characterization of fiber reinforced composite material. *New Chem. Mater.* **2022**, *50* (1), 15−19.

https://doi.org/10.1021/acsomega.3c05728
ACS Omega 2023, 8, 39984−40004

(15) Su, Y.; de Rooij, M.; Grouve, W.; et al. The effect of titanium surface treatment on the interfacial strength of titanium−Thermoplastic composite joints. *Int. J. Adhes. Adhes.* **2017**, *72*, 98−108.
(16) Critchlow, G. W.; Brewis, D. M. Review of surface pretreatments for titanium alloys. *Int. J. Adhes. Adhes.* **1995**, *15* (3), 161−172.
(17) Molitor, P.; Barron, V.; Young, T. Surface treatment of titanium for adhesive bonding to polymer composites: a review. *Int. J. Adhes. Adhes.* **2001**, *21* (2), 129−136.
(18) Goushegir, S. M.; dos Santos, J. F.; Amancio-Filho, S. T. Influence of aluminum surface pre-treatments on the bonding mechanisms and mechanical performance of metal-composite single-lap joints. *Welding in the World* **2017**, *61* (6), 1099−1115.
(19) Wen, H. B.; De Wijn, J. R.; Cui, F. Z.; et al. Preparation of bioactive Ti6Al4V surfaces by a simple method. *Biomaterials* **1998**, *19* (1−3), 215−221.
(20) Bezek, K.; Nipic, D.; Torkar, K. G.; Oder, M.; Drazic, G.; Abram, A.; Zibert, J.; Raspor, P.; Bohinc, K. Biofouling of stainless steel surfaces by four common pathogens: the effects of glucose concentration, temperature and surface roughness. *Biofouling* **2019**, *35* (3), 273.
(21) Grujicic, M.; Sellappan, V.; Omar, M. A.; et al. An overview of the polymer-to-metal direct-adhesion hybrid technologies for load-bearing automotive components. *Journal of Materials Processing Technology* **2008**, *197* (1−3), 363−373.
(22) Rohart, V.; Lebel, L. L.; Dubé, M. Improved adhesion between stainless steel heating element and PPS polymer in resistance welding of thermoplastic composites. *Composites Part B: Engineering* **2020**, *188*, No. 107876.
(23) Wang, P. *Study on Bonding Properties of Interface Modified Stainless Steel/Polyolefin Composite Tape for Optical Fiber*; Hubei University of Technology, 2019.
(24) Li, J. *Study on the Preparation of Stainless Steel/CFRTP Components by Mixed Copunching*; Yanshan University, 2021.
(25) Ghosh, A. K.; Bertels, E.; Goderis, B.; et al. Optimisation of wet chemical silane deposition to improve the interfacial strength of stainless steel/epoxy. *Appl. Surf. Sci.* **2015**, *324*, 134−142.
(26) Li, X.; Sun, M.; Song, J.; et al. Enhanced adhesion between PEEK and stainless-steel mesh in resistance welding of CF/PEEK composites by various surface treatments. *High Perform. Polym.* **2021**, *33* (8), 892−904.
(27) Yang, M. *Conductive Properties of ABS/Stainless Steel Fiber Composites*; Hubei University of Technology, 2015.
(28) Jiang, B. L.; Bai, L. J.; Jiang, Y. F. The Technique of Microarc Oxidation on Aluminum Alloy. *J. Xi'an Univ. Technol.* **2000**, *02*, 138−142.
(29) Zhao, J. *Research on micro-arc oxidation process of stainless steel and its mechanism of bonding with resin*; Southwest Jiaotong University, 2019.
(30) Zhou, J F. *Study of amine-modified epoxy resin adhesives*; Guilin University of Technology, 2007.
(31) Zhou, J. F.; Li, A.; Rao, B. L. Effect of Metal Surface Treatment and Bonding Technology on Shear Strength. *Chem. Adhes.* **2007**, *29*(1), 30−32, 43.
(32) Ni, S.; Sun, L.; Ercan, B.; et al. A mechanism for the enhanced attachment and proliferation of fibroblasts on anodized 316L stainless steel with nano-pit arrays. *Journal of Biomedical Materials Research Part B: Applied Biomaterials* **2014**, *102* (6), 1297−1303.
(33) Bouquet, F.; Cuntz, J. M.; Coddet, C. Influence of surface treatment on the durability of stainless steel sheets bonded with epoxy. *J. Adhes. Sci. Technol.* **1992**, *6* (2), 233−242.
(34) Gaillard, F.; Romand, M. Surface characterization of AISI 304L stainless steel subjected to various prebonding treatments. Correlation with adhesion measurements. *Surf. Interface Anal.* **1988**, *12* (9), 491−496.
(35) Zhao, P. *Design and mechanism of resistance welding interface enhancement of thermoplastic aerospace composites*; Shenyang Aerospace University, 2020.
(36) Xiong, X.; Zhao, P.; Ren, R.; Zhang, Z.; Cui, X.; Ji, S. Effect of chemical etching of resistance wire surface on the strength and failure mechanism of the resistance-welded joint of polyetherimide composites. *J. Appl. Polym. Sci.* **2019**, *136* (34), 47879.
(37) Kwon, M. Y.; Lee, S. G. Analysis of the Interfacial Adhesion between a Stainless-Steel Fiber and an Epoxy Resin by the Single Fiber Microdroplet Test. *Surfaces* **2020**, *3* (4), 594−604.
(38) Van Rooijen, R. G. J.; Sinke, J.; Van Der Zwaag, S. Improving the adhesion of thin stainless steel sheets for fibre metal laminate (FML) applications. *J. Adhes. Sci. Technol.* **2005**, *19* (16), 1387−1396.
(39) Baniya, H. B.; Guragain, R. P.; Subedi, D. P. Cold atmospheric pressure plasma technology for modifying polymers to enhance adhesion: A critical review. *Progress in Adhesion and Adhesives* **2021**, *6*, 841−879.
(40) Chen, S.; Ono, S.; Teii, S.; et al. Improvement of the adhesion of the resin to the metal surface by using plasma jet. *Surf. Coat. Technol.* **1997**, *97* (1−3), 378−384.
(41) Schutze, A.; Jeong, J. Y.; Babayan, S. E.; Park, J.; Selwyn, G. S.; Hicks, R. F. The atmospheric-pressure plasma jet: a review and comparison to other plasma sources. *IEEE Transactions on Plasma Science* **1998**, *26* (6), 1685−1694.
(42) Hu, Y., Lv, R. D., Liu, G. J.; et al. *Physical Chemistry*, Version 5; Higher Education Press: Beijing, 2007: pp 486−490.
(43) Tang, P.; Liu, L. X.; Cao, D. P.; et al. Review on Adhesion Mechanism and Adhesion Enhancement of Organic Coatings. *Mater. Protection* **2020**, *53* (02), 126−135.
(44) Wang, C.; Li, Y.; Tong, L.; et al. The role of grafting force and surface wettability in interfacial enhancement of carbon nanotube/carbon fiber hierarchical composites. *Carbon* **2014**, *69*, 239−246.
(45) Xiong, X.; Wang, D.; Ren, R.; et al. Enhancement of thermosetting composites resistance welding by carbon nanotubes. *J. Qingdao Univ. Sci. Technol. (Nat. Sci. Ed.)* **2021**, *42* (5), 54−61.
(46) Xiong, X.; Wang, D.; Wei, J.; et al. Resistance welding of thermoplastics by carbon nanotube-grafted heating element. *J. Adhes. Sci. Technol.* **2021**, *35* (16), 1806−1819.
(47) Zhang, C.; Lin, H.; Zhang, S.; Xie, Q.; Ren, C.; Shao, T. Plasma surface treatment to improve surface charge accumulation and dissipation of epoxy resin exposed to DC and nanosecond-pulse voltages. *J. Phys. D: Appl. Phys.* **2017**, *50* (40), 405203.
(48) Ochoa-Putman, C.; Vaidya, U. K. Mechanisms of interfacial adhesion in metal−polymer composites−Effect of chemical treatment. *Composites Part A: Applied Science and Manufacturing* **2011**, *42* (8), 906−915.
(49) Williams, T. S.; Yu, H.; Yeh, P. C.; et al. Atmospheric pressure plasma effects on the adhesive bonding properties of stainless steel and epoxy composites. *J. Compos. Mater.* **2014**, *48* (2), 219−233.
(50) Chen, Q. L.; Du, B.; Zhang, X. D.; et al. Parametric Investigation into the Shear Strength of Adhesively Bonded Single-Lap Joints. *Materials* **2022**, *15* (22), 8013.
(51) Kim, M. C.; Yang, S. H.; Boo, J. H.; et al. Surface treatment of metals using an atmospheric pressure plasma jet and their surface characteristics. *Surf. Coat. Technol.* **2003**, *174*, 839−844.
(52) Wang, B.; Bai, Y.; Hu, X.; et al. Enhanced epoxy adhesion between steel plates by surface treatment and CNT/short-fibre reinforcement. *Compos. Sci. Technol.* **2016**, *127*, 149−157.
(53) Zhu, D.; Qin, Y.; Huang, Q.; et al. Improvement of adhesion performance between modified phenolic and stainless steels by titanate coupling agent treatment. *J. Adhes. Sci. Technol.* **2020**, *34* (7), 782−791.
(54) Jiang, C.; Che, Z.; Xing, F.; et al. Research progress on interlaminar property of carbon nanotube-continuous fiber reinforced resin matrix composites. *Acta Mater. Composit. Sin.* **2022**, *39* (03), 863−883.
(55) Fan, Z.; Santare, M. H.; Advani, S. G. Interlaminar shear strength of glass fiber reinforced epoxy composites enhanced with multi-walled carbon nanotubes. *Composites Part A: Applied science and manufacturing* **2008**, *39* (3), 540−554.

https://doi.org/10.1021/acsomega.3c05728
ACS Omega 2023, 8, 39984−40004

(56) Qian, H.; Greenhalgh, E. S.; Shaffer, M. S. P.; et al. Carbon nanotube-based hierarchical composites: a review. *J. Mater. Chem.* **2010**, *20* (23), 4751−4762.
(57) Sharma, V. K. Influence of amine functionalized multi-walled carbonnanotubes on the mechanical properties of carbonfiber/epoxy composites. *Mater. Today Proceed.* **2021**, *37*, 2978−2981.
(58) Baltzis, D.; Orfanidis, S.; Lekatou, A.; et al. Stainless steel coupled with carbon nanotube-modified epoxy and carbon fibre composites: Electrochemical and mechanical study. *Plastics, Rubber and Composites* **2016**, *45* (3), 95−105.
(59) Arai, S.; Kawahito, Y.; Katayama, S. Effect of surface modification on laser direct joining of cyclic olefin polymer and stainless steel. *Materials & Design* **2014**, *59*, 448−453.
(60) Sun, A.; Liu, M.; Dong, Q. Prediction of tensile strength for short-fiber-reinforced composites. *Chin. J. Mater. Res.* **2008**, *03*, 333−336.
(61) Yu, Z.; Bai, Y.; Li, Y.; et al. Fiber length distribution and thermal, mechanical and morphological properties of thermally conductive polycarbonate/chopped carbon fiber composites. *Polym. Int.* **2018**, *67* (8), 1137−1144.
(62) Qu, P.; Wan, Y.; Bao, C.; et al. A new numerical method for the mechanical analysis of chopped carbon fiber tape-reinforced thermoplastics. *Composite Structures* **2018**, *201*, 857−866.
(63) Cui, X.; Zhao, P.; Xiong, X.; et al. Enhancement of chopped fibers on welding strength of composites. *J. Mater. Eng.* **2019**, *47* (12), 151−156.
(64) Shi, J.; Yao, R.; Kong, Z.; et al. Strength analysis on hybrid welding interface of polymer and short carbon fiber reinforced composite. *J. Mater. Sci.* **2021**, *56* (26), 14556−14569.
(65) Liu, B. Study on Technology of Epoxy Modified Silicone Resins. *Paint Coatings Industry* **2008**, *12*, 26−29.
(66) Zou, H.; Chen, Y.; Zhang, C.; et al. Enhancing the mechanical properties of fiber metal laminate by surface treatment. *Polym. Compos.* **2023**, *44* (4), 2080−2092.
(67) Zhang, Y.; Hasegawa, K.; Kamo, S.; et al. Enhanced adhesion effect of epoxy resin on metal surfaces using polymer with catechol and epoxy groups. *ACS Appl. Polym. Mater.* **2020**, *2* (4), 1500−1507.
(68) Scarselli, G.; Quan, D.; Murphy, N.; et al. Adhesion improvement of thermoplastics-based composites by atmospheric plasma and UV treatments. *Applied Composite Materials* **2021**, *28* (1), 71−89.
(69) Nishikawa, M.; Okabe, T.; Hemmi, K.; et al. Micromechanical modeling of the microbond test to quantify the interfacial properties of fiber-reinforced composites. *International Journal of Solids and Structures* **2008**, *45* (14−15), 4098−4113.
(70) Liu, R.; Liang, D. Interface Study of Smart Composite Material with Optical Fiber by Single-Fiber Pull-Out Test. *Chin. J.Lasers* **2009**, *36* (02), 387−390.
(71) Zhu, D.; Yao, M.; Zhang, H.; et al. Temperature effect on the mechanical properties of CFRP/Steel single-lap shear joints under dynamic tensile loading. *China Civil Eng. J.* **2016**, *49* (08), 28−35.
(72) Liu, G.; Yang, F.; Bai, Y.; et al. Enhancement of bonding strength between polyethylene/graphene flakes composites and stainless steel and its application in Mode IV storage tanks. *Journal of Energy Storage* **2021**, *42*, No. 103142.
(73) Chen, Z.; Peng, Y.; Li, C.; et al. Experimental study for the adhesive interface mechanical properties of double lapped steel-CFRP plate at high temperature. *Acta Mater. Composit. Sin.* **2021**, *38* (02), 449−460.
(74) Gao, X.; Zang, Y.; Xu, F.; et al. Hygrothermal aging effects on double lap shear joints of composite laminates. *Chin. J. Appl. Mech.* **2021**, *38* (05), 2042−2048.
(75) Dubé, M.; Chazerain, A.; Hubert, P.; et al. Characterization of resistance-welded thermoplastic composite double-lap joints under static and fatigue loading. *Journal of Thermoplastic Composite Materials* **2015**, *28* (6), 762−776.
(76) Xie, W. *Finite Element Analysis of Interfacial Stresses of Cracked Steel Structure Strengthed with CFRP Plate*; Guangdong University of Technology, 2016.
(77) Wang, S. *Research on Mode I Fracture Performance of Carbon Fiber/Steel Composite Structure*; Chang'an University, 2020.
(78) Liu, W.; Jiao, G. Mode I interlaminar fracture toughness for Z-pins reinforced C/SIC composites. *Chin. J. Solid Mech.* **2013**, *34* (05), 466−472.
(79) Chandrasekaran, S.; Sato, N.; Tölle, F.; et al. Fracture toughness and failure mechanism of graphene based epoxy composites. *Compos. Sci. Technol.* **2014**, *97*, 90−99.
(80) Sharma, P.; Mali, H. S.; Dixit, A. Mechanical behavior and fracture toughness characterization of high strength fiber reinforced polymer textile composites. *Iranian Polymer Journal* **2021**, *30* (2), 193−233.
(81) Ding, J. C.; Xu, W. Determination of mode I interlaminar fracture toughness of composite by a wedge-insert double cantilever beam and the nonlinear J integral. *Compos. Sci. Technol.* **2021**, *206*, No. 108674.
(82) Luo, J. *Study on Mode-II Fracture Properties of Carbon Fiber/Steel Composite Structure Reinforced by Short Fibres*; Chang'an University, 2019.
(83) Almansour, F. A.; Dhakal, H. N.; Zhang, Z. Y. Investigation into Mode II interlaminar fracture toughness characteristics of flax/basalt reinforced vinyl ester hybrid composites. *Compos. Sci. Technol.* **2018**, *154*, 117−127.
(84) Barbosa, L. C. M.; Bortoluzzi, D. B.; Ancelotti, A. C., Jr Analysis of fracture toughness in mode II and fractographic study of composites based on Elium® 150 thermoplastic matrix. *Composites Part B: Engineering* **2019**, *175*, No. 107082.
(85) Gliszczynski, A.; Wiącek, N. Experimental and numerical benchmark study of mode II interlaminar fracture toughness of unidirectional GFRP laminates under shear loading using the end-notched flexure (ENF) test. *Composite Structures* **2021**, *258*, No. 113190.
(86) Pennas, D.; Cantwell, W. J. The influence of loading rate on the mode III interlaminar fracture toughness of composite/steel bi-material systems. *Journal of composite materials* **2009**, *43* (20), 2255−2268.
(87) Audd, C.; Davidson, B. D.; Ratcliffe, J. G.; et al. Reexamination of the edge crack torsion test for determining the mode III delamination toughness of laminated composites. *Engineering Fracture Mechanics* **2019**, *215*, 138−150.
(88) Bertorello, C.; Viña, J.; Viña, I.; et al. Study of the influence of the Mode of matrix used in carbon-epoxy composites on fatigue delamination under mode III fracture. *Materials & Design* **2020**, *186*, No. 108345.

https://doi.org/10.1021/acsomega.3c05728
ACS Omega 2023, 8, 39984−40004